HIGH SPEED CONTINUOUS ADDITIVE MANUFACTURING AT THE LIQUID-LIQUID INTERFACE

A Thesis

Presented to the Faculty of the Graduate School

of Cornell University

In Partial Fulfillment of the Requirements for the Degree of

Master of Science

by

Laura Elena Montoya Ashton

May 2018

ABSTRACT

This work investigates stereolithography at a liquid-liquid interface. The first working curves printed at a liquid-liquid interface are presented and closely match those printed at liquid-solid interfaces. A model describing the curing behavior at a liquid-liquid interface is derived and suggests that print speeds up to 162 cm/hour are possible with a commercially available resin. Resin cure speeds of 159 cm/hr and prototype system print speeds of 81 cm/hr were demonstrated using liquid-liquid interface stereolithography. The suitability of various aqueous, organic, and fluorinated organic liquid subphases are evaluated based on UV transmission, environmental considerations, immiscibility, spreading behavior, density, and chemical compatibility with the resin. High quality single-layer prints can be produced on multiple subphases. Print quality decreases for 3D prints due to capillary effects at the interface. The trade-off between resin spreading and subphase wetting at the print interface is explored.

BIOGRAPHICAL SKETCH

Laura Elena Montoya was born to a long line of proud New Mexicans. After graduating in the Top 10 students from Sandia High School, she attended the New Mexico Institute of Mining and Technology because she had heard it was the hardest school in the state. Four years later, she graduated summa cum laude and married Ryan Ashton.

Her B.S. in chemical engineering and minor in explosives engineering were put to good use during the two years she spent as a Ballistics Engineer at a specialty oil field supply company. She left after three patent applications and establishing her own pyrotechnics laboratory for an opportunity to further her education in a fulltime capacity.

She started graduate studies at Cornell University in the fall of 2016 and served first as an Outreach Chair and then as President of the Graduate Society of Women Engineers. She will graduate with a M.S. in mechanical engineering in May 2018 and move back to New Mexico as a Member of the Technical Staff at Sandia National Laboratories.

To my dearest Ryan, without whom this thesis would never have been completed, thank you.

To my parents, Catherine and Randy, and sister, Amanda, I hope I represented us well.

In loving memory of Lorenza R. Montoya (September 1918-May 2017).

ACKNOWLEDGMENTS

The author wishes to thank and acknowledge Sandia National Laboratory's Critical Skills Master's Program for funding this work; Dr. Hanrath for his instruction, inspiration, and advice which were essential to this thesis; Dr. Shepherd for his expert knowledge of the field, recommendation of textbooks, and careful review of this thesis; and to Dr. Cook and Dr. Hirschfeld for reviewing this thesis for public release.

Sandia National Laboratories is a multi-mission laboratory managed and operated by National Technology & Engineering Solutions of Sandia, LLC, a wholly owned subsidiary of Honeywell International Inc., for the U.S. Department of Energy's National Nuclear Security Administration under contract DE-NA0003525.

The views expressed in this document do not necessarily represent the views of the U.S. Department of Energy or the United States Government.

This document went through the formal Review and Approval process and was approved for UUR by SAND No: SAND2018-4815 T.

TABLE OF CONTENTS

LIST OF FIGURES

LIST OF TABLES

LIST OF ABBREVIATIONS

ABS	Acrylonitrile butadiene styrene
AD	Autodesk
AM	Additive manufacturing
CAD	Computer aided design
CANFI	Continuous Additive Nanomanufacturing at Fluid Interface
CLIP	Continuous Liquid Interface Production
CMOS	Complementary metal oxide semiconductor
CNC	Computer numerical control
DI	Distilled water
DLP	Digital light projector
DMD	Digital micromirror device
EBM	Electron beam fusion
FDM	Fused deposition modeling
FFF	Fused filament fabrication
IR	Infra-red
LCD	Liquid crystal display
LOM	Laminated object manufacturing
MEMS	Micro-electrical-mechanical-system
MJ	MakerJuice
PBF	Powder bed fusion
PI	Photo initiator
PLA	Polylactic acid
SDS	Safety data sheet

SLM	Selective laser melting
SLS	Selective laser sintering
SM	Subtractive manufacturing
STL	File type used for stereolithography
TI	Texas Instruments
UV	Ultra violet

BODY OF THESIS

CHAPTER 1

INTRODUCTION

A Brief History of Humans Making Things

Humans have been using tools for millennia. The evolution of civilization is a story of technological advancements. Many tools are used to make new tools. Each advance cracked the door open a little wider for future advances. Therefor the history of societal growth is enabled by the development of more sophisticated tools and the ability to make more intricate products.

Subtractive Manufacturing

For centuries, the main process for making durable products has been through various methods of subtractive manufacturing. As its name implies, subtractive manufacturing (SM) is based on the principle of removing material from a larger piece to make a final, smaller part. SM applications range from Clovis man's fluted projectile points painstakingly chipped from volcanic glass some 11,500 years ago [1], to medieval craftsman carving molds for casting iron wares [2], and to modern machine shops capable of "lights out" manufacturing using 5 or more axis milling machines [3].

Subtractive manufacturing techniques have been refined over the centuries and are now quite versatile. Humans landed on and returned from the Moon using only SM methods. However, SM has several limitations and drawbacks which will be discussed further here. SM requires a block of material at least as big as the desired final part [4]. Think of making a wooden bowl. A piece of wood at least as tall and wide as the bowl

is needed from which it will be carved. Most of the wood will end up as small, wasted turnings and sawdust as only a thin section of the original block is present in the final bowl. Thankfully, wood is abundant and inexpensive. Now imagine using a CNC milling machine (computer numerical control) to make a thin, arching airfoil from an expensive and rare metal alloy. The material waste is now a significant consideration. Further picture the labor involved in changing the airfoil design. Perhaps the airfoil is changed to a hollow design to reduce weight and now must be manufactured as separate parts and things like how the parts will join must be further considered. Additionally, the CNC machine will have to be reprogrammed, a process that one source described as "very involved" [4]. As the airfoil example illustrated, there are certain geometries like internal features, square holes, and some undercuts that SM techniques cannot achieve and keep the design as a single part [4]. These weaknesses in SM eventually gave rise to the idea for an entirely new way to think about making things: additive manufacturing.

Additive Manufacturing

Additive manufacturing (AM) is a relatively new method of making parts but already has several key advantages over SM techniques. Its invention is most commonly attributed to the 1984 patent of Charles Hull, an American, entitled "Apparatus for production of three-dimensional objects by stereolithography" [4], [5]. While Hull is most often credited, similar patents were filed at nearly the same time by individuals from France and Japan [4]. AM fundamentally changes the way parts are made by gradually adding small amounts of material that accumulate to build up a part instead of removing material as is the case with SM. This difference in mechanism allows for

a greater range of geometries that can be achieved with minimal or no extra effort for increased complexity [4]. AM excels at making undercuts and internal features. AM can literally print a ‘ship inside a bottle’ in a single step while [4]. The more complex the geometry, the more difficult, time intensive, and, often, expensive it is to make with SM methods. In contrast, the geometry complexity is inconsequential to the print speed and cost for many types of AM [6]. If the design changes, a new CAD (computer aided design) file is simply uploaded to the AM machine and it prints the part [4]. (Types of AM techniques will be discussed in detail below.) Another advantage of AM is that it reduces raw material waste which has become a reason for companies to invest in furthering the development of these technologies [7]. Up to 96% of the starting material can be removed during the subtractive manufacturing of a part [8]. While the exact amount of material saved is dependent on the part geometry, Petrovic reports an average material savings of 40% with 95%-98% of the waste being recyclable for metal applications [9]. AM’s ease of accommodating changing and complex designs, ability to make undercuts and internal features in a seamless part, and reduction of raw material consumption have made it a technology worthy of further study but have not yet enabled it to displace SM on a large scale.

Initially, applications for AM were limited to making design models and curios. AM gained popularity primarily through its use to produce prototypes, markups, and small, complex, highly customizable parts like dental implants [6]. The ease of going from a CAD file to physical part in a matter of hours with in-house capacities was attractive to many companies. The material costs were comparable to more traditional methods but the near elimination of material waste and dramatic reduction of skilled labor

needed to produce a part made the overall production of a part competitive with or cheaper than SM techniques. There was also an added benefit to many companies that did not have full in-house SM capabilities and had historically needed to send designs out for prototyping and fabrication. Now those companies could reduce the risk of designs being leaked to competitors by using AM to keep their prototyping process internal to the company [7].

The fundamental differences in approach of AM and SM result in interesting economic implications and niche market dominance based on the relationship of production quantity, time to delivery, if the design is finalized or subject to either changes or many variations, and material property requirements. AM is expected to become a disruptive technology akin to digital music and eBooks [7]. Part of the attraction is that AM can allow companies to both reduce unsold inventories and serve smaller market segments like dental and medical, replacement parts, prototypes, and even bridge manufacturing by providing small quantity production runs of complex items [6], [7]. Additionally, AM enables a company to be agile, a necessary characteristic as competitive advantages are known to be transient [10].

Perhaps the potential of AM was most famously stated by then-President Barak Obama during his 2013 State of the Union Address when he said that “3D printing…has the potential to revolutionize the way we make almost everything” [11].

Commercially Important Types of Additive Manufacturing

Over the past decades, the several AM technologies have matured while an abundance of new techniques continue to be developed. A selection of some of the more mature,

commercially viable methods for AM are discussed in this section in order from obvious to imaginative.

Laminated Object Manufacturing

During laminated object manufacturing (LOM), a continuous roll of thin stock material is unwound across the top of the build area where a laser traces the cross section's outline to cut out the layer [12]. The layer is then attached through either an adhesive or welding process to the previous layers of the part before the roll unspools further and a new cross section is cut using the laser [13]. A popular adhesive method is to use a heat activated adhesive on the underside of the material [14]. Capabilities currently exist for using up to 5 rolls of material, which can have different thicknesses, compositions, and material properties, during the build process [12]. One or more of these rolls maybe used to deposit support materials to assist in the production of overhangs and internal features.

Materials for LOM

A variety of materials ranging from paper [4] to ceramics [12] to plastics [15] and to metals [13] can be used to make a 3D object using LOM. The primary limiting factor to the materials that can be used is that a uniform foil of the material that is wrapped into a roll must be able to be made [13]. The layer-binding mechanism, vertical resolution, and dimensional accuracy is dependent on the material and method used. The three main methods of layer-binding are gluing or adhesion bonding, bond-then-form, form-then bond. Using a paper-backed tape is a simple way to visualize printing with and adhesive and papers as thin as 70 μm have been used in LOM [4]. Metal foils

can also be used with an adhesive backing and can have a lateral accuracy of 120 µm [13]. In a bond-then-form process, the sheet of material is bonded to the lower layer before being cut to shape with the laser. This bonding is most commonly achieved by using a heated roller to activate a thermally initiated bond [4]. As could be inferred, the cross section is first cut free from the roll and carefully aligned with the lower layers before bonding in a form-then-bond process. Parts made using both bond-then-form and form-then-bond processes typically need a post-process heating step to prevent delamination. This post-process heating can cause 12 to 18% shrinkage which leads to dimensional in accuracies and, sometimes, delamination of the layers [12], [15].

Applications of LOM

LOM has primarily been used for making models and prototypes as it tends to have a staircase effect on the edges, which can be reduced by using thinner layers at the expense of print speed, and highly anisotropic mechanical properties [4]. One niche that LOM seems "cut out for" is making channels for microfluidic devices [12].

Extrusion-based Methods

The first patent on an extrusion-based 3D printing method went to Scott Crump of Stratasys Inc. in 1989 for [16]. Crump is also attributed with coining the name Fused Deposition Modeling (FDM) to describe this method of depositing thin layers of "solidifying material until the shape is formed" [16]. Since the phrase FDM was determined to be protected as part of the patents so later companies adopted the term Fused Filament Fabrication (FFF) for the same process using a polymer or

thermoplastic filament [17]. The general process of FDM or FFF is to slice a computer model into layers that are relayed to the 3D printer that moves either the extrusion nozzle or the build stage laterally to draw the layer. When a layer is complete, the build stage moves down to allow space for the next layer [15]. The filament is moved to the heated, temperature controlled extrusion nozzle by motorized rollers. Any variation in the diameter or density of the filament can result in gaps in the printed part or jamming of the nozzle [18]. Care must be taken when printing small layers to ensure the deposited material has cooled enough to solidify before depositing the next layer and small fans are often incorporated into the printer for this purpose. The staircase and chordal effects of the model slicing to accommodate for the layer thickness are signatures of this method [15].

Materials for Extrusion-based Printing

Extrusion-based 3D printing benefits from having a large diversity of materials that it can process. The types of materials that can be printed with extrusion methods are classified as either melting based extrusion, as is the case for the polymers and thermoplastics used in FFF, or are based on a chemical change which includes solvent-based extrusion [4]. The later relies on some form of chemical change to cause solidification and this can include a reaction with air, an internal curing reaction, or simply the evaporation of water or another solvent [4]. Materials that have been successfully printed with this method include electromagnetic bandgap materials [19], cement [20], concentrated (50 to 65%) colloidal ceramic slurries [12], fiber reinforced composites [21], silicon nitride, fused silica, piezoelectric ceramics, tungsten carbide composites, alumina, and even metals like stainless steel [18]. For melting processes,

plastics with an amorphous structure produce better prints than highly crystalline ones as a viscous paste is better for extrusion. This is due to lack of a distinct melting point for amorphous polymers which causes them to become increasing soft and supple with increasing temperature instead of transitioning directly from a solid to a lower viscosity liquid [4]. Advanced printers that can change the printed material mid-print have even been developed to give more user control of the part's properties [15].

Supports and Support Material

There are many geometries like undercuts and overhangs that must be supported during the extrusion-based 3D printing process. Supports are printed to help keep the part's intended shape and can be made from either the same material as the part or a secondary material [4]. If the same material as the part is used in the supports, careful consideration must be given to the print design so that the supports can be removed without damaging the part once the print is finished. It is easier to remove supports when they are made from a different material than the printed part as differences in the material properties can be exploited. Differences can be achieved by printing a higher porosity or lower grade of the same material or by printing a dissimilar material that can be selectively dissolved with a solvent [4].

Applications of Extrusion Printed Parts

Today, the uses of 3D printed parts are difficult to keep abreast of as ideas and technology advance snowball into new innovations. Some of the current applications of extrusion printed parts include electronic sensors [22], scaffolds for tissue engineering [23], reaction ware for selective chemical synthesis [24], bionic ears [25],

microfluidic devices [26], metal-pipe rectangular guides for microwaves [27], and even a bridge for cyclists [28]. While an all-inclusive list would have to be updated as soon as it was completed, this one is meant to be representative of the diverse applications being pursued with this technology.

Extrusion-based 3d printers have the distinction of being the most popular with hobbyists [4], partially due to their low price point. A current, entry-level model can be purchased for around $200 from many big box stores like Best Buy [29], Staples [30], Office Depot [31], and Walmart [32]. These printers extrude melted PLA (polylactic acid) or ABS (acrylonitrile butadiene styrene) filaments in thicknesses down to 100 µm and with an x- y- resolution of down to 400 µm for just $150 [32]. While the majority of parts made using FDM or FFF are used as models, prototypes, or curios, there an increasing number of functional products [33], [34]. One of the many uses of 3D printed products has been to make more 3D printers in a self-replicating process. The idea of having a machine that is capable of making copies of itself can be dated back over 50 years to John von Neumann [35]. Today, businesses like RepRap work to advance the percentage of components that 3D printers can make for use in making more 3D printers with the goal of one day becoming a true von Neumann machine [17].

Powder Bed Fusion

Powder bed fusion (PBF) devices are among the oldest types of 3D printers and use a thermal source to fuse powder particles. The original idea for a PBF is attributed to Carl Deckard who, in 1984, was an undergraduate at the University of Texas at Austin [36]. PBFs operate by using a computer controlled thermal source such as a laser or,

less commonly, an electron beam to fuse loose powder into a cohesive part [4]. A pre-heating step is often used to raise the temperature of the powder to a sub-fusing level to increase the efficiency of the laser or electron beam. Once a single layer has been fused, a fresh layer of powder is dispensed and leveled before the process repeats [36]. The powder that is not incorporated into the part acts as support material and is removed at the end [15]. Metal powders, polymer dusts, and ceramics have all been successfully printed using PBF techniques [12], [4], [15]. PBF techniques require the material to have a known melting point and well-defined phase transition so crystalline polymers and pure metals are easier to process than amorphous plastics and alloys [4]. While there are nearly infinite variations of PBF techniques and devices, a few of the more commercially significant are discussed below.

Selective Laser Sintering and Melting

Selective laser sintering (SLS) and selective laser melting (SLM) are two closely related AM techniques that also build an object in a layer-by-layer method, this time via the utilization of a high powered laser to heat a powder with fine particle size [12]. Between layers in both techniques, a fresh layer of loose powder is spread over the top of the part [37]. Typical layer thickness is 75 to 100 μm and an inert gas atmosphere can be used to decrease powder oxidation, degradation, and waste [4]. Modern embodiments of both SLS and SLM use heaters to keep the powder at an elevated, uniform temperature to reduce the necessary laser power, laser projection time, and internal part stresses that can cause warping [4]. The x- y- resolution is limited to 50 to 200 μm and is dependent on the powder properties and machine used [38].

The primary difference between the two techniques is that SLM fully melts the particles into a homogeneous part while SLS provides just enough energy to fuse the surfaces of adjacent particles [37], [39]. While SLS and SLM are similar both in name and method, the resulting material properties can be quite different. SLS is a solid-state process and is performed at a lower temperature and does not melt the powder particles but is instead driven by the minimization of total free energy [4]. SLS tends to produce parts with higher porosity and poorer mechanical properties than SLM although the degree of porosity and resulting properties can be controlled via process parameters like particle surface area and laser scan rate [4], [40]. Its parts are prone to shrinkage and frequently require a postprocessing annealing to prevent warping [4], [38], [40]. SLM fully melts the powder and can produce parts with up to 99.9% maximum density but is also limited in the materials that it can print [38]. Because an alloy's melting point is a function of its composition, SLM cannot be used with raw alloys as constituent particles of different metals have different melting points and will change the concentration in the melted material from the bulk concentration [38]. However, if the powdered alloy particles are of homogeneous molecular composition, SLM can be used and the unique properties that arise from the rapid melting and setting of the part can "be more desirable than cast or wrought parts made from identical alloys" [4].

Applications of SLS and SMS

Aerospace companies have helped drive the development of SLS and SMS techniques. The reduced material waste, ability to make previously impossible geometries in a single part, and cost efficiency of making small production runs helped to attract

investments from the likes of Boeing and Lockheed Martin [41]–[43]. The first 3D printed structural part to pass intensive quality tests and fly as part of a military aircraft was a titanium pylon in 2003. The pylon was made by Boeing at the request of the Air Force Research Laboratory for the F-15 fighter jet via SLM when a replacement part was needed and the tooling lead time was determined to be too long. Today, there are over 50,000 3D printed components in Boeing-made aircraft alone [41].

Electron Beam Melting (EBM)

EBM is similar to other PBF methods in that it melts or sinters a thin layer (50 to 200 μm) of preheated particles in a powder in order to gradually build up a part [44]. As the name suggests, an electron beam is used as the heat source. The beam is generated from a high voltage electron gun and is then focused by electromagnetic lenses before being directed by a magnetic scan coil [45], [46]. The beam current and scanning speed are adjusted to achieve either sintering or melting. The materials best suited to EBM are electrically conductive which prevents its use on most ceramics and polymers. If a full melt is desired, the layer is first lightly sintered to immobilize the particles as they are susceptible to charging and repulsion before the beam makes a second pass to fully fuse the layer [46]. Once a layer is complete, a fresh layer of powder is deposited and the next slice from a computer generated model is traced out. In contrast to SLS and SLM which use an inert gas atmosphere to print, EBM operates under vacuum (less than 10^{-4} Torr) to prevent beam scattering [47]. If the material properties of the powder require it, the pressure can be increased to approximately 10

Torr by using helium although this is known to increase part cooling and heat conduction [47].

Similarities of EBM and SLM

Both techniques have difficulty printing the first layer of an overhanging feature due to the loose powder having a lower thermal conductivity than the solid, metallic part. This causes hot spots which can cause distortion [48].

Stereolithography

Stereolithography (SL [12], [49]–[52] although SLA is also used in the literature [6], [53]–[56]) was the first form of AM to be commercialized with the original patent awarded to Charles Hull in 1984 [5]. This layer-by-layer approach to building an object takes a computer generated design file as its input which is then sliced into cross sections for projecting into a photo-curable liquid resin bath [12]. In the years since 1984, the complexity and diversity of SL devices on the market has increased nearly exponentially. A Google Scholar search for the term 'stereolithography,' excluding citations, limited to publications from 2016-2017 returns 16,200 results of which some 6,500 are patents [57]. Some of the most significant variants are discussed below.

Evolution of Projection Methods

There are multiple ways to provide the light energy necessary for initiating polymerization of the SL resin. Progress in this area has been largely driven by technological advances in the fields of optics and micromanufacturing. This discussion is limited to UV light sources as these are the most commercially important category

but everything from gamma and x- rays to visible light has been used to cure specialty resins [4].

Laser

In laser-based SL applications, sometimes called “vector scans” [4] or “vector-by-vector” printing [58], layers are cured by rastering the beam across the photopolymer. This method can yield objects with a high resolution in the x- and y- directions but is limited by the diameter of the laser beam. Laser-based SL can be time consuming as the laser must trace the entire profile for every layer and there is a maximum linear velocity of the trace above which insufficient energy will be imparted and the resin will not cure. To improve print speed, solid parts are often printed with a few cured internal supports and fully cured edges, leaving the majority of the internal resin as an uncured liquid. After the print process, the object is placed in a post-process UV oven to finish curing the internal resin. While this increases the printer’s throughput, this method can cause warping and shrinkage [15].

Projection and Masking

Significant time can be saved over vector scanning methods by using a projector and mask to cure an entire layer of resin in a single exposure [12]. Originally, masks were physical objects that had to be made into the shape of each layer to block part of the projected light. Whenever the projected cross section needed to change, the mask had to be removed and another installed [5]. By 1997, liquid crystal displays (LCD) were used to dynamically generate masks [59]. While LCDs were a huge improvement over physical masks, they were limited to a “low switching speed (~20 ms), large pixel

sizes, low filling ratio, low optical density of the refractive elements during the off mode, and the higher light absorption during the on mode" [12], [60]. These limitations lead to the development of the digital dynamic masking methods discussed in the next section.

DMD in DLPs

Digital micromirror devices (DMD) are arrays of up 8 million individually controllable reflective micromirrors [61]. They are a type of micro-electrical-mechanical system (MEMS) that convert an electrical input from a CMOS (complementary metal oxide semiconductor) memory cell into optical output using aluminum micromirrors. Each micromirror is responsible for projecting a single pixel and can be cycled between the highly repeatable on and off states to produce grayscale patterns [61].

DMDs represent a significant improvement over LCD masks as modulation efficiency was improved from 12.5% via transmission for LCD to 88% via reflection for DMD, pixel size was reduced from 33 μm to about 15 μm, and the switching speed dropped from 20 ms to 20 μs [60], [62].

Digital light projection (DLP) systems use DMDs to control the projection of light into a liquid resin bath. DLPs are the complete projector system while DMDs control what portions of the light from a source within the DLP gets projected as an image. DLPs can use any light source of sufficient power and wavelength to initiate resin polymerization. Sources representing the portion of the spectrum from ultraviolet (UV) to infrared (IR) with wavelengths from 363 nm to 2500 nm are currently on the

market [61]. The majority of stereolithography applications require UV for resin curing.

Materials for Stereolithography

Polymers and Epoxies

UV curable polymers and epoxies are the most common materials for use in stereolithography and are discussed in depth in the next chapter. Both the polymer and epoxy resins tend to be thermosetting, that is they form irreversible cross-links during the curing process.

Novel Materials for SL

There are on-going research efforts print more diverse materials with SL techniques. These efforts have included using acoustic fields to pattern metallic nanoparticles dispersed in polymer resins to create simple circuits [63] and ceramic nanoparticles with photo-excitable ligands to create parts that approach the mechanical properties of conventional shaping methods [53].

Applications

Photopolymers have been used commercially since the late 1960s for applications that do not require patterning including coatings for paper products and dental sealants [4]. Since the invention of SL, it has been used to make countless prototypes and models in addition to objects as diverse as micro-machines [12], scaffolds for heart valve tissue [54], [64], plastic injection molding cavities [65], and self-healing soft robots [66]. As the speed and available materials increase, the applications of SL are expected to continue growing.

Next Generation SL Technologies

There are many next generation SL techniques being published today. Some use electric or acoustic fields to align particles in the resin into patterns [63]. Others seek to print novel materials like nano-composites [53]. This paper presents a new technique for dramatically increasing the print speed of SL.

Continuous Liquid Interface Printing (CLIP)

In 2015, the CLIP method of 3D printing very quickly with SL made scientific headlines with both a *Science* paper [49] and a TED Talk [67]. CLIP used oxygen inhibition, a long-time nuisance to SL, as a feature. By projecting through the bottom of an oxygen permeable glass and into the resin, they prevent the resin from adhering to the glass as the polymerization reaction is prevented from progressing near the window due to the high oxygen concentration. They named this layer where oxygen inhibits polymerization the "dead zone." The presence of a dead zone allows for the printed part to be drawn out of the resin without the need to peel each layer off of the glass which results in a significant time savings. CLIP boasts print speeds of 50 cm/hr [49] which is about 27 times faster than conventional methods [68]. The maximum print speed of the CLIP method is limited by the ability to keep oxygen in the dead zone. As the print speed increases, the thickness of the dead zone decreases until the resin is eventually able to polymerize all the way to the glass bottom and cause a print jam.

Continuous Additive Nano-manufacturing at the Fluid Interface (CANFI)

The CANFI method is similar to CLIP in that it is also a continuous process as it prevents layer adhesion to the bottom and is capable of rapid print speeds. However,

the CANFI method uses a liquid-liquid interface instead of an oxygen permeable glass to prevent adhesion and achieve rapid print speeds. Floating the resin on a dense, UV transmissive subphase, enables fast, continuous printing that is not limited by the diffusion rate of oxygen. By taking advantage of the same mechanical printing mechanism as CLIP but removing the chemical limitation of oxygen diffusion, CANFI has the potential to achieve print speeds in excess of 162 cm/hr, or to exceed conventional SL print speed by 90 times.

CHAPTER 2

THE SCIENCE OF STEREOLITHOGRAPHY

In Depth Look at Photopolymers

Polymers

Polymers are a class of materials that are composed of many smaller, linked sub-units called monomers. Polymers can be both naturally occurring, as is the case for DNA, or synthetic, like the polyethylene used to make a disposable water bottle. Both natural and synthetic polymers are composed primarily of carbon and hydrogen in addition to frequently containing oxygen and nitrogen. Their long, chain-like structures yield large molecular masses even though the constituent atoms are relatively light. Due to their cumbersome structure, they rarely form crystals but are instead prone to forming semi-crystalline or amorphous structures.

Polymers can have different structures as a result of the way they were made and their chemical makeup. Thermoplastic polymers, which are used in both injection molding and some extrusion based AM techniques, tend to have branching or linear molecular structures [4], [69]. These polymer structures result in the ability to repeatedly melt and solidify [4]. The polymers used for SL differ from thermoplastics in their structure, formation mechanism, and material properties. The polymers used in SL rely on a crosslinking mechanism to form which is discussed in detail in a later section. In crosslinked systems, molecular movement within the solid polymer is more restricted than in linear or branched systems. This structural rigidity increases with the

degree of crosslinking and results in physical rigidity. Crosslinked polymers tend to be both harder and more brittle than thermoplastics and have higher melting points [70]. Additionally, they do not re-solidify with the same chemical composition and material properties after melting which makes them unfavorable for use in extrusion AM or injection molding but perfectly serviceable for SL applications [4].

The present discussion is limited to chain growth systems as these have out competed step growth systems in the commercial market due to a combination of many factors that include faster cure rates and lower volatile organic content [65], [71].

Resin Constituents: Monomers, Oligomers, Photoinitiators Initiators, Reactive Diluents, and UV Blockers

There are many components in modern resins that serve a variety of purposes. Not every component is present in every resin and often specialty chemicals are added to modify the behavior or properties. All resins contain some form a chemical "building blocks" and another chemical that can cause the blocks to link together to form larger blocks. These building blocks can be either monomers or oligomers and are frequently a mixture of both. A monomer is a relatively small molecule that can bind to other identical monomers to form a polymer. Oligomers have been defined as "radiation curable binders" [72] and are molecules that are larger than a monomer but smaller than polymer. The variety of molecular weights, and resulting proprieties like increased viscosity, available in oligomers allow a resin to have more tailored properties than by using only monomers [73]. Both monomers and oligomers can be made to polymerize by reacting with a photoexcited photoinitiator (PI). PI are present

at all times in the resin but only become reactive once they have been photoexcited to either a free radical or ionic state [4], [69]. Strong absorption in the range of the light source's wavelength(s) and fast kinetics are desirable properties for PIs whose role it is to rapidly convert the energy of the incident light into chemical energy [74].

If the viscosity of the resin is too high (10,000 cps is common) once a monomer and/or oligomer and PI have been selected, it may be necessary to add a diluent to reduce the viscosity to about 100 cps [75]. Diluents are carefully chosen such that they can partake in the polymerization reaction, are commonly referred to as reactive diluents, have a low molecular weight, and can be used to improve mechanical or optical properties [73].

If a high print fidelity is desired in a part that does not have a continuously solid body but instead contains cutouts or overhangs, then it may be necessary to incorporate a UV blocker [76], sometimes called a UV absorber [60], into the resin formulation. UV blockers adjust the curing depth to prevent the over-curing of a previously printed layer by reducing light scattering and absorption depth [60], [77].

Polymerization Reactions

Chain Growth vs Step Growth

Polymer growth can occur in either a stepwise manner, which includes the historic categories of condensation and addition, or by chain growth. In chain growth reactions, monomer concentration steadily decreases as units are added onto an activated polymer chain [71], [78]. During chain growth reactions, high molecular weight chains form throughout the reaction whereas they form only near the end of a

step growth reaction [71].It is therefore possible to achieve large molecular weights in relatively short times using chain growth. The following discussion will be limited to chain growth systems as this is the type of reaction occurring during stereolithography and encompasses both ionic and free radical induced polymerization [78], [79].

Free Radical Systems

A molecule need only to contain a carbon-carbon double bond in order to serve as a monomer in free radical polymerization processes [79]. This allows a wide variety of chemistries to be used and, typically, milder reaction conditions than are needed for other methods like ionic polymerization. As this thesis is being filed with the Mechanical and not the Chemical Engineering Department, the author will borrow the generalized reaction mechanism from Reed and Alb's book in Figure 1, below.

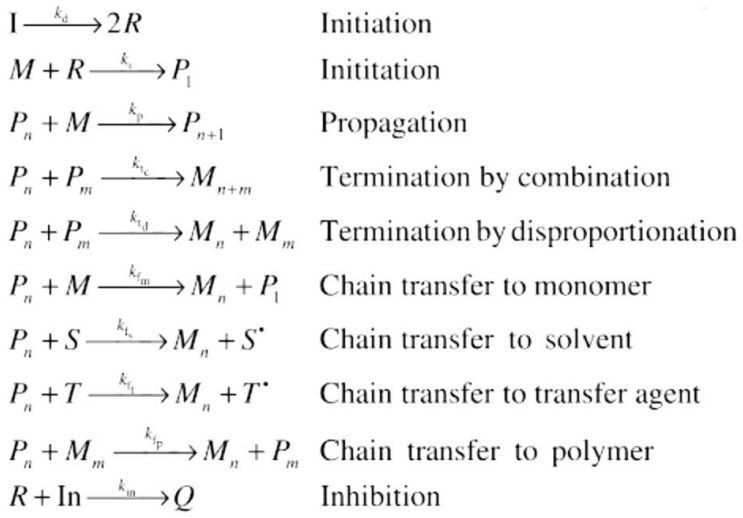

Figure 1: Mechanism of free radical induced polymerization where the photoinitiator (I) interacts with light to form radicals (R) that interact with the monomer (M) to form a polymer (P) as presented by Reed et al. [79]**.**

When thinking about the rate at which this simplified model polymerizes, it is necessary to consider the probability of polymerization (α) occurring once a free radical is formed. Free radical formation does not necessarily have to lead to polymerization as losses to the surroundings, solvent, and oxygen inhibition can remove radicals from the system. For systems where oxygen inhibition is not significant, as would be the case if using an inert atmosphere or bottom projection method, the polymerization rate can be related to the monomer (M) and photoinitiator (I) concentrations, probability of polymerization (α), and reaction chemistry specific constant (k) [4], [79], [80].

$$R_p = \left|\frac{d[M]}{dt}\right| \qquad \textbf{Eqn. 1}$$

Polymerization stops when two radicals neutralize each other without joining, two polymer chains combine by joining two radicals, or the radical sites get blocked from further reactions by the solidifying polymer preventing fresh monomers from reaching the site. These are termination mechanisms are referred to as disproportionation, recombination, and occlusion, respectively [4].

Excitation Energy

Photoinitiators (PI) require a minimum energy in order to become a reactive species capable of inducing the polymerization of monomers. If a photon's energy is less than the minimum energy needed by the PI, it will not form a reactive species and polymerization will not occur. Since energy is inversely proportional to wavelength, photons with wavelengths above some maximum value will not be able to induce

polymerization. Therefore, most resins can be worked with in an interior but well-lit laboratory without unintended reactions despite being light activated as UV is not present (although there are some resins that have been specially formulated to react with visible light [4]) [65]. An appropriate PI must be selected based on the light source's wavelength. The power of the laser or light source can be much lower than other AM techniques with typical powers of 10 mW to 1 W [65].

Oxygen Inhibition

Oxygen from the air can diffuse and dissolve into the liquid resin. Oxygen preferentially reacts with active PI and eliminates radicals before they can initiate polymerization. It can be so severe that some resins cannot be printed with top projection in air and can cause print failure if using a very thin layer of resin with bottom projection.

Ionic Systems

Epoxy based resins are the most common ionic systems although other systems like vinylethers have niche commercial markets [4]. Unlike free radical polymerization that has interactions at the covalent pi-bonds of a carbon-carbon double bond, ionic systems react at sites along a carbon ring [4]. A distinct advantage of ionic systems is their intrinsic insensitivity to the presence of oxygen [78]. Unlike free radical systems, ionic systems can continue limited polymerization even after the light source has been shuttered once ionic species are produced [78]. This can be a beneficial for the reduction of projection time as the part will continue to cure after active exposure but can have negative impacts on dimensional accuracy if the part is left in the resin bath.

Acrylate Based Resin Systems

Acrylate based resin systems were the first to be developed and undergo free radical initiation to form long polymer chains. They build linearly once the photoinitiator has been light activated to link monomers into long segments. Cross linking does not occur until the polymer chains have grown enough that they impinge on another chain's space [4]. While they react quickly to UV radiation they also are prone to warping and curling as a result of shrinkage [4]. However, their low viscosity assists with spreading between layers, they have a low critical energy, and are relatively insensitive to changes in both temperature and humidity which are all desirable characteristics [81].

The research presented in this thesis utilized two different commercially available polymers: the G+ resin from MakerJuice Labs [82] and the Standard Clear Prototyping Resin (PR48) from Autodesk [83]. Both systems use acrylate based chemistries and are free radical systems. The compositions of both systems, hereafter referred to as MJ and AD for the MakerJuice Labs' G+ resin and Autodesk's Standard Clear Prototyping Resin (PR48), respectively, as reported on the manufacturers' safety data sheet (SDS) are show below in Table 1.

Table 1: Compositions of Two Commercial Acrylate Resins [82]–[85]

Manufacturer	MakerJuice Labs		Autodesk	
Product Name	G+		Standard Clear Prototyping Resin (PR48)	
Maximum Curing Wavelength (nm)	420		~ 410	
Purpose	Chemical Name/ Description	Concentration	Chemical Name/ Description	Concentration

Photo Initiator	Not Reported	< 1 wt%	2,4,6-Trimethylbenzoyl-diphenylphosphineoxide) Esstech TPO+	0.4 wt%
Oligomers			Alkoxylated pentaerythritol tetraacrylate/ Allnex Ebecryl 8210 and Sartomer SR 494	39.776 wt% each
Reactive Diluent & Monomer	Acrylate Ester	> 60 wt%	Aliphatic Urethane Acrylate/ Rahn Genomer 112	19.888 wt %
UV Blocker			2,2'-(2,5-thiophenediyl) bis(5-tertbutylbenzoxazole/ Mayzo OB+	0.160%

Epoxy Based Systems

Epoxy based systems are worth noting as they have important specialty applications. They exhibit much smaller shrinkage than acrylate based systems, with 1-2% shrinkage possible [4], [86]. This is due to epoxies breaking open a ring in order to react so that the quantity and types of bonds present changes minimally before and after reaction [87]. Epoxies do not strictly follow the polymerization rate that was discussed above as they continue to react even after the light source has been removed [4]. Epoxies react more slowly than acrylate systems and new resins are being formulated that try to take advantage of the fast reaction rate of acrylates while maintaining the low shrinkage of epoxies [88].

Critical Exposure and Gel Point

It is helpful to distinguish the interrelated terms used to describe light. Table 6 in APPENDIX 1 contains definitions, symbols, and disambiguation of the terms used in this section.

Someone new to SL might assume that by shortening the exposure time or using a reduced dosage, they would achieve a thinner cured thickness. They would be right up until a critical point below which the resin will not cure. It is, unfortunately, not possible to achieve an infinitely thin film by using an infinitely short exposure time. Instead, there is as minimum critical exposure (fluence, not just energy) that must be imparted to bring the liquid resin to its gel point and to form a solid layer. This gel point, which occurs at the critical exposure (E_{crit}), is an innate property of the resin and will vary from resin to resin. The minimum layer thickness of the cured resin also happens at E_{crit} and is dependent on the type of resin used.

Light Attenuation and Absorption

Resins gradually attenuate UV light as it is absorbed by the photoinitiator and, if present, the UV blocking agent. By combining Beer's and Lambert's Laws, a relationship between absorbance (A), absorptivity (ε), concentration (c), and path length (b) can be obtained [89].

$$A=\varepsilon bc \qquad \textbf{Eqn. 2}$$

Rewriting Eqn. 2 in terms of the absorption coefficient at the wavelength of interest (α) and by using z to denote vertical path through the resin instead of b, the Beer-Lambert Law becomes

$$A = \alpha c \int_0^z \mathrm{d}z \qquad \textbf{Eqn. 3}$$

.

While the resin's affinity for absorbing photons (α) remains constant throughout the system, the number of photons (Φ) that are present decrease exponentially as the depth

into the resin and distance from the light source increase (see Eqn. 6). This results in the exponential decrease in the quantity of photons absorbed (A) with increasing depth (z) as shown below.

$$\frac{dA}{dt} = -\alpha A \qquad \textbf{Eqn. 4}$$

$$A(z) = A_0 e^{-\alpha z} \qquad \textbf{Eqn. 5}$$

$$\Phi(z) = \Phi_0 e^{-\alpha z} \qquad \textbf{Eqn. 6}$$

Comparable to the time constant in a resistor-capacitor circuit, it is helpful to define the penetration depth (D_p) of a resin as the depth (z) at which the flux drops to 1/e of the incident amount, or about 37% of Φ_0.

$$D_p = {}^{1}/_{\alpha} \qquad \textbf{Eqn. 7}$$

$$\Phi(D_p) = \Phi_0 e^{-\alpha D_p} = {}^{\Phi_0}/_{e} \qquad \textbf{Eqn. 8}$$

It is convenient to convert Eqn. 6 into a relationship involving the exposure (E, units of mJ/cm^2) as this is what can be easily measured experimentally. Equations Eqn. 23, Eqn. 24, Eqn. 6, and Eqn. 7 combine to give

$$\mathrm{E}(z) = \mathrm{E}_0 e^{{}^{-z}/_{D_p}} \qquad \textbf{Eqn. 9}$$

.

It was previously established that a resin requires some critical exposure (E_{crit}) to cure. For any incident exposure (E_0) less than the critical exposure, no polymerization will occur. E_{crit} serves as a minimum threshold below which the exposure is inconsequential. The maximum practical exposure, an E_{max}, can be defined as the

exposure above which no additional resin will cure due to absorption. Both E_{crit} and E_{max} have values specific to a given resin.

The application of the above relationships to the speed of curing and printing through a working curve are discussed in the next section.

Speed of SL

The speed of a stereolithographic process is dependent on both the available light energy and the material properties. An approach to determining the maximum print speed from the available light energy and experimentally determined resin properties is discussed below.

Working Curves

The ubiquitous working curve [4], [49], [55], [60], [62], [65], [90]–[93] relates the cured depth (C_d, also called the thickness of the cured layer) to exposure as shown below.

$$E_{max}(z) = E_{crit}\, e^{-z/D_p} \qquad \textbf{Eqn. 10}$$

$$C_d = D_p \ln\left(\frac{E}{E_{crit}}\right) \qquad \textbf{Eqn. 11}$$

Equation Eqn. 11, which is the traditional form of the "working curve equation," is just a rearranged version of equation Eqn. 10 where i) a generic E that is both less than E_{max} and greater than E_{crit} and ii) it is assumed that for depths (z) in this range the resin will cure (C_d). From this working curve equation, the relationship between C_d and the applied E can be graphed with a linear relationship on a semi-logarithmic plot with a slope equal to D_p and an intercept at E_{crit}, giving us the gel point. In this model, both

D_p and E_{crit} are purely parameters of the resin and independent of the power of the light source [93].

Reaction Rates

Currently, there is no single quantitative model that can analytically predict photopolymerization reaction rates although several models can be applied to specific systems and experimental parameters [4], [80], [94], [95]. While a model that fully captures the behavior photopolymerization reactions and chemistries is elusive, some simple relationships have been explored. In a simplified system where only photoinitiator (I) and monomer (M) react to form a polymer (P), the polymerization rate (R_p) is equivalent to the rate of monomer consumption as shown below [4], [80].

Reaction $M+I \rightarrow P$

$$R_p = -\frac{dM}{dt} = \alpha M(kI)^{1/2} \qquad \textbf{Eqn. 12}$$

It can be observed from Eqn. 12, where k is a constant, that the reaction rate is directly proportional to the monomer concentration but only scales by the square root of the photoinitiator concentration [4], [80].

Print Direction

Top-Down

In this variation of SL, the light source is located below the resin and it passes through a UV transparent window in the bottom of the resin reservoir. Historically, this has meant that every newly cured layer adheres to the glass at the bottom of the reservoir and the part must be delaminated from the glass before a new layer can be printed. The flow of the printing cycle can be thought of as expose the resin, separate from the

glass, and repeat with the exposure taking up 30 to 70 % of the cycle time, depending on the resin's photosensitivity and viscosity [96]. The separation of the freshly cured photopolymer from the glass must overcome Stefan Adhesion, the force required to separate two disks in a viscous fluid [96], [97]. This force is a function of the resin viscosity (μ), the separation velocity (υ), the characteristic length (l), height between the two disks (h), and time (t) as shown in Eqn. 13. For the 3D printing case of two disks, the printed layer and bottom of the vessel, the characteristic length is the radius and it is more consistent to think of height in the z-direction which gives Eqn. 14.

$$F \propto \mu v \frac{l^4}{ht^3} \qquad \textbf{Eqn. 13}$$

$$F = 3\pi\mu v \frac{r^4}{2z^3}\frac{dz}{dt} \qquad \textbf{Eqn. 14}$$

Over the years, many approaches have been used to overcome Stefan Adhesion to peel the freshly cured layer of resin from the bottom of the printing vessel. A schematic from Adzima's presentation of some of these separation mechanisms is shown below.

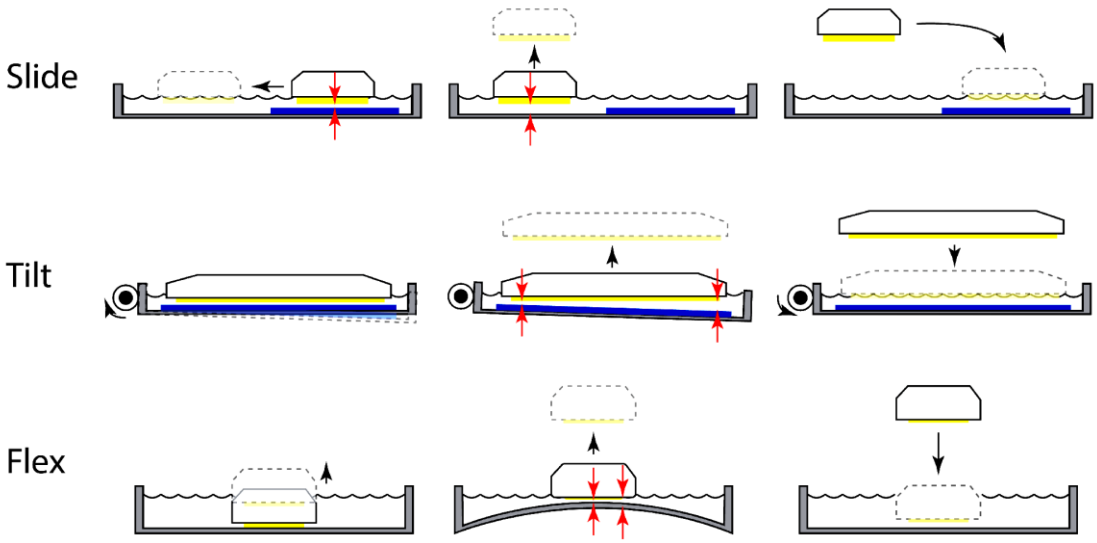

Figure 2: Mechanisms for separating cured resin layers from the window as presented by Adzima [96]**.**

The act of peeling the cured layer from the bottom exerts a tension force on each layer of the 3D object. This tugging action can reduce the mechanical properties compared to part that did not experience these stresses, such as one printed with a bottom-up method [4].

Bottom-Up

The bottom-up printing method uses top-illumination to project an image down onto the resin from above. After the layer has cured, the build stage lowers farther into the resin bath so that fresh resin can flow onto to the top of the cured layer. The DLP projects a new layer, the build stage steps lower, fresh resin covers the top of the part, and the process repeats. The print height is limited by the size of the resin reservoir and this method is not conventionally feasible for printing resins that are scarce. While little resin is wasted during this print method, a large amount of resin is required so that it can cover the entire printed part as it submerges into the bath. Oxygen inhibition of polymerization at the top surface of the resin can negatively impact print quality and speed. Oxygen from the surrounding air is partially soluble in most resins and will preferentially react with the free radicals from activated PIs during illumination. This quenches the polymerization reaction near the surface. In systems with low light penetration and high oxygen diffusion, this can cause total print failure by preventing polymerization entirely. In less severe cases, the print speed is merely reduced as the height of the cured layered for a given exposure is reduced from what the resin is capable of without oxygen inhibition. Modern systems that use top-illumination will

use a resin that is not susceptible to oxygen inhibition or apply an inert atmosphere like nitrogen.

A potential advantage to using a top-illumination system is the buoyant forces exerted by the resin on the printed part could reduce the need for printed supports in some geometries.

Resolution of SL

There are many factors that can impact a system's print resolution and over the years some creative methods have been developed, including shrinking a printed object up to 80% during a post-processing pyrolysis step [98], to achieve ever smaller features. It is important to note that this thesis will focus on positive printed features and their resolution. If the reader is interested in resolution of producing negative spaces and controlled voids, the recent paper by Gong et. al. on making microfluidic channels presents a systematic study of the topic [99].

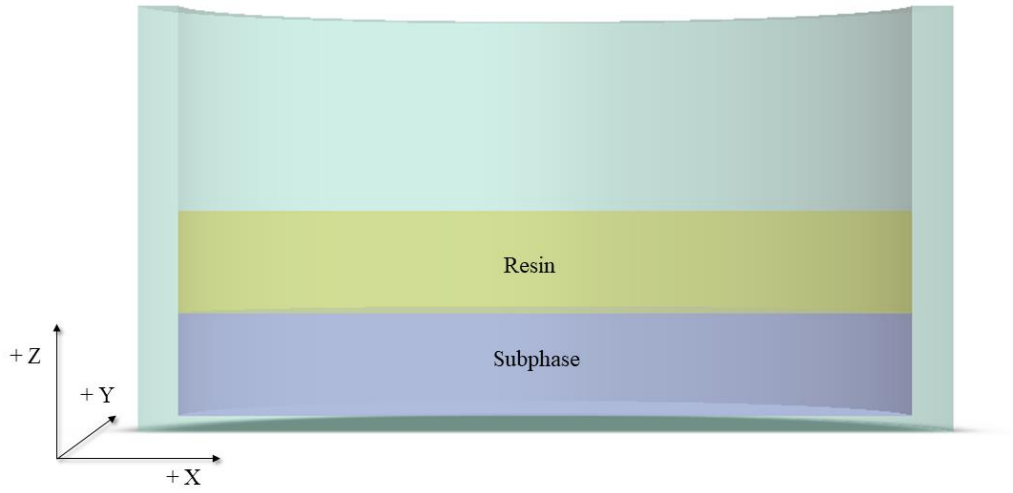

Figure 3: Cross sectional view of the liquid resin and subphase in a transparent vessel (shown in green) with the x-, y-, and z- axes.

Lateral

The print resolution in the x- and y- directions (see Figure 3, above) is impacted both by the material properties of the resin and by the specifications of the light source. Photopolymer based resin systems need the polymerized chains to reach a minimum length and level of cross linkage in order to have mechanical robust enough to allow the printed parts to be measured and handled. When the polymer chains are too short, the material properties decline. The minimum cured width is not significantly improved by adding a UV blocker is low exposures are used [60].

Light becomes increasing diffuse due to its diffractive nature that farther from the source it travels according to the point-spread function [100]. Texas Instruments (TI) is the primary manufacturer of DMDs [12], [60], [61], [76], [91] and the smallest reported lateral feature attained using their systems is a 0.6 μm diameter suspended beam [60]. For comparison, a commercial DLP printer like Autodesk's Ember can achieve a resolution of about 50 μm [76], [91]. Further improvement of lateral resolution may be possible by projecting subvoxel sized gray-scale images by oscillating a single DMD mirror between the on and off states during a projection [91].

Vertical

Resolution in the z-direction (see Figure 3, above) is dependent on the minimum layer thickness that can be cured. Historically, this has been limited by the motor that moves the build stage [4]. In theory, a stereolithography system using a liquid subphase could achieve a smaller vertical displacement than even a stepper motor utilizing micro-stepping by adding or removing a small but precise volume of subphase to a large diameter reaction vessel. For example, envision a syringe pump using a small diameter

syringe whose extrusion is being controlled by a mechanical displacement system. The syringe dispenses additional subphase into a reaction vessel with a diameter many times that of the syringe. The dispensed liquid's volume is spread by gravity across the entire reaction vessel. The improvement in vertical resolution over mechanical displacement will scale as square of the vessel's radius over the square of the syringe's radius. This advance has the potential to improve the vertical resolution to be approximately equivalent or superior to the lateral resolution which has historically been finer due to being limited by the DMD instead of mechanical stepping [4], [60]. There is a third way to control to control the vertical resolution. In addition to mechanical displacement and changing the thickness of the subphase, the height of the cured layer can be controlled by either the exposure or by addition of a UV blocker [60]. Both UV blockers and reduced exposure time can be used to make a thinner layer of cured resin. While the author could not find published results on any system using this method, it is theoretically possible to expose the resin for a short time, less than that required to form the maximum thickness of a single layer, in order to cure a very thin layer of resin. The limitation to photo-controlled method is that it can only be used to create a single layer and would not be useful for a multi-layer part production as the cured layer would be free standing at the liquid-liquid interface separate from the build head.

Projection Edge Effects

It is important to keep the projection edge effects in mind when designing an experiment. Jacobs provides an excellent analysis of the effects in a system using a laser as the light source [93]. Similar effects are observed when using a DLP but the

scan speed falls out of the equations and the exposure can be used instead. If a thin line is projected with width L_W (or a laser with beam width L_W), the resin cured in that single layer will not be a perfect rectangular prism as might be expected. Instead, the cured width tapers off gradually until the maximum cured depth (z_{max}) beyond which no resin solidifies.

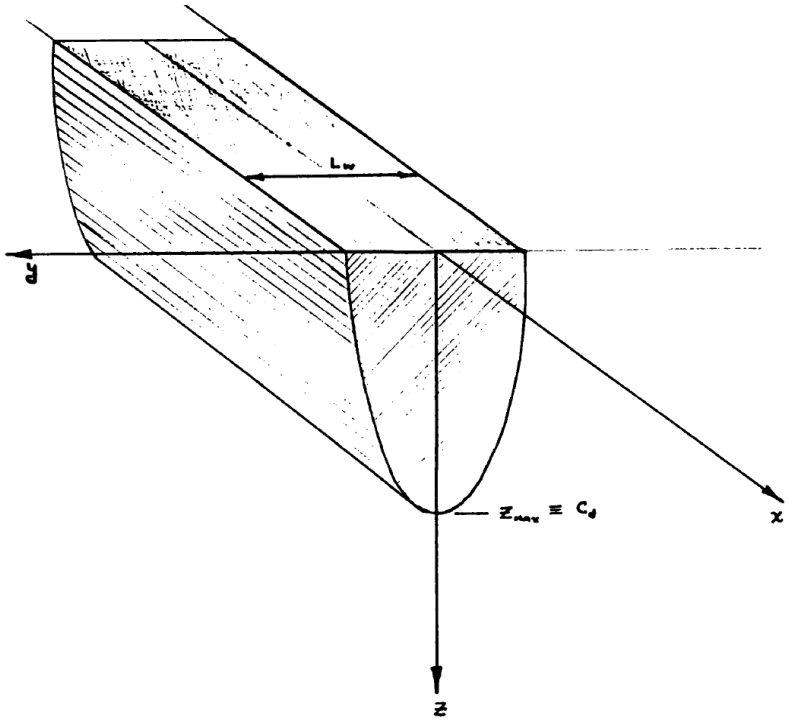

Figure 4: Edge effects caused by absorbance within a single cured layer as presented by Jacobs [85]**.**

Typically, this effect is not macroscopically visible in parts made using a DLP as the entire sheet is cured instantaneously and so this effect is only significant at the edges of the cured layer. However, this can become significant when a thick layer or a feature with a very small cross section is printed and is visible under an optical microscope [63].

Shrinkage

While a few technologies rely on shrinkage phenomena achieve smaller feature size [98], shrinkage is typically viewed as an inconvenience in SL. Acrylate based resins typically shrink by 5-20% [86] which can cause poor adhesion, warping, curling, and part failure [4]. The timescale for the onset of shrinkage can be "orders of magnitude" longer than the exposure time and, for acrylate systems, are normally complete after about 10 s [4].

CHAPTER 3

CONSIDERATIONS AND RESULTS OF PRINTINIG AT THE LIQUID-LIQUID INTERFACE

Experimental Setup

The primary experimental setup used the light source, USB-to-computer interface, and z-direction stepper motor from Autodesk's Ember 3D printer. The printer's settings were modified via an SSH connection to stop the tray from rotating and to override the magnetic positioning sensors and jam detector. Additional print and projection related settings were changed directly through Autodesk's PrintStudio interface. By physically removing the resin tray, slider, original build head, and the outer plastic housing, it is possible to install a custom printing vessel and build head with an adjustable height build stage as shown in Figure 5.

The DLP projects a cross sectional image for a set time interval onto a UV reflective mirror and through the bottom of the borosilicate reaction vessel. The UV light then travels through the liquid subphase before being absorbed in the resin where it triggers a chemical reaction that creates a solid layer. Once the layer has cured, the build stage raises and the next cross section is projected. Note that no separation method like sliding or over-lifting and then lowering the printed part is needed as the freshly printed layer does not adhere to the liquid subphase as it would to a solid substrate or window.

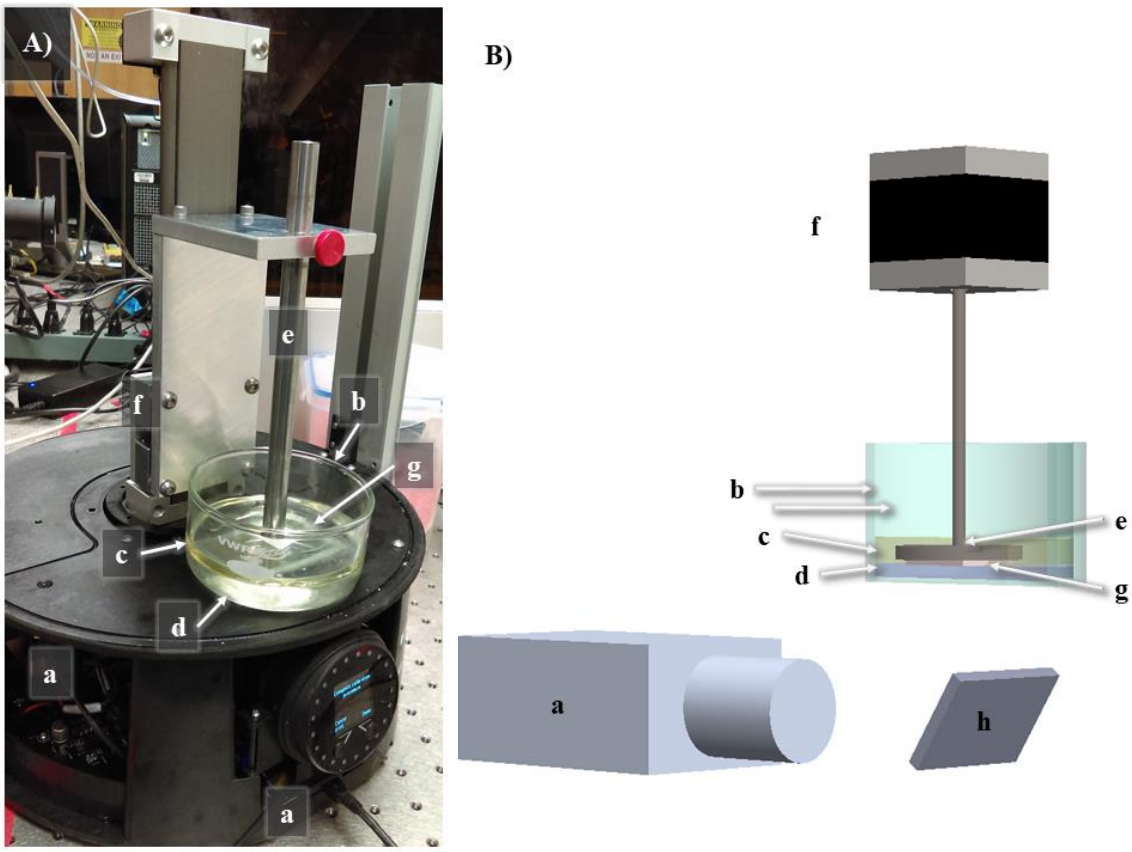

Figure 5: Experimental setup (A) and CAD model (B) of the top-down printing method where a) is the DLP, b) is the borosilicate reaction vessel, c) is the resin, d) is the subphase, e) is the build head and shaft attaching it to f) the stepper motor or mechnical displacement device, g) is the solidfied resin that makes the 3D printed object, h) is the mirror (not visible in the physical setup), and i) is the computer interface port.

Print Direction

Different factors must be considered when printing at a liquid-liquid interface as there are different challenges and benefits to each approach.

Top-Down

The absorptivity of the print vessel and subphase must be carefully considered in a top-down printing configuration (see Figure 5, above) as both can reduce the amount of light reaching the resin. Additionally, it is important to maintain a constant subphase height or take the changing absorbance into consideration as this will affect the light available to the resin. It is helpful to think of an effective incident exposure. While E_0 is the exposure incident to the bottom of the print vessel, $E_{0,\,eff}$ is the amount reaching the bottom of the resin after passing through the print vessel and subphase. This is discussed further in the UV Transmission section below but, in summary, about 88% of E_0 becomes $E_{0,\,eff}$ with most of the losses originating from the use of a borosilicate glass reaction vessel and not from the subphase.

The thickness of the resin layer is another parameter that should be intentionally controlled. Depending on the desired material and print properties, anywhere between a monolayer (tens of nm) to more than 10 cm of resin can be used. The case for a desiring a monolayer is made by groups who do nanomaterial work as the self-assembly of highly ordered lattices of particles at a liquid-liquid interface has been demonstrated [101]. The case for a thick layer of resin is supported by the need to minimize oxygen inhibition and to assist in resin spreading to replace the curing material. By using a layer of resin thicker than the diffusion length of oxygen into the resin, the effects of oxygen inhibition at the liquid-liquid interface are minimized without the need for an inert atmosphere. The effects of gravity's pressure head on spreading is explored in a later section on surface energy effects.

Unlike conventional top-down printing, the cured resin layer cannot bond to the bottom but instead is suspended by the liquid subphase. While Stephan Adhesion is still relevant to raising the solidified layer from the interface, the magnitude of the force necessary is greatly reduced and the printed object is expected to have better mechanical properties as a result of the reduction of this force [50]. The part can be lifted straight up without a complex separation mechanism which will reduce the time needed to process each layer and increase print speed.

Bottom-Up

While this thesis focuses primarily on bottom-illumination, the CANFI approach can be used with top-illumination to reduce the amount of resin needed to print a part by eliminating the need for the reservoir to filled with resin. Instead, a thin layer of resin, just greater than the volume of the final part, can be spread on top of a liquid subphase. The printed part lowers over the course of the print cycle into the subphase instead of into a deep resin reservoir. This method of printing was actually described in Charles Hull's original 1984 patent [5]. The support provided by the buoyant forces is increased in this method as the subphase has a higher density than the resin. It is possible that certain geometries would need fewer support structures vs the quantity needed for top-down printing. An inert atmosphere is needed for bottom-up print setups as the printing is occurring at the resin-air interface and the oxygen from the air can inhibit polymerization of the top layers of resin.

The UV transmittance of the subphase is unimportant in a bottom-up configuration as the light does not need to penetrate the subphase in order to reach the photopolymerizable resin.

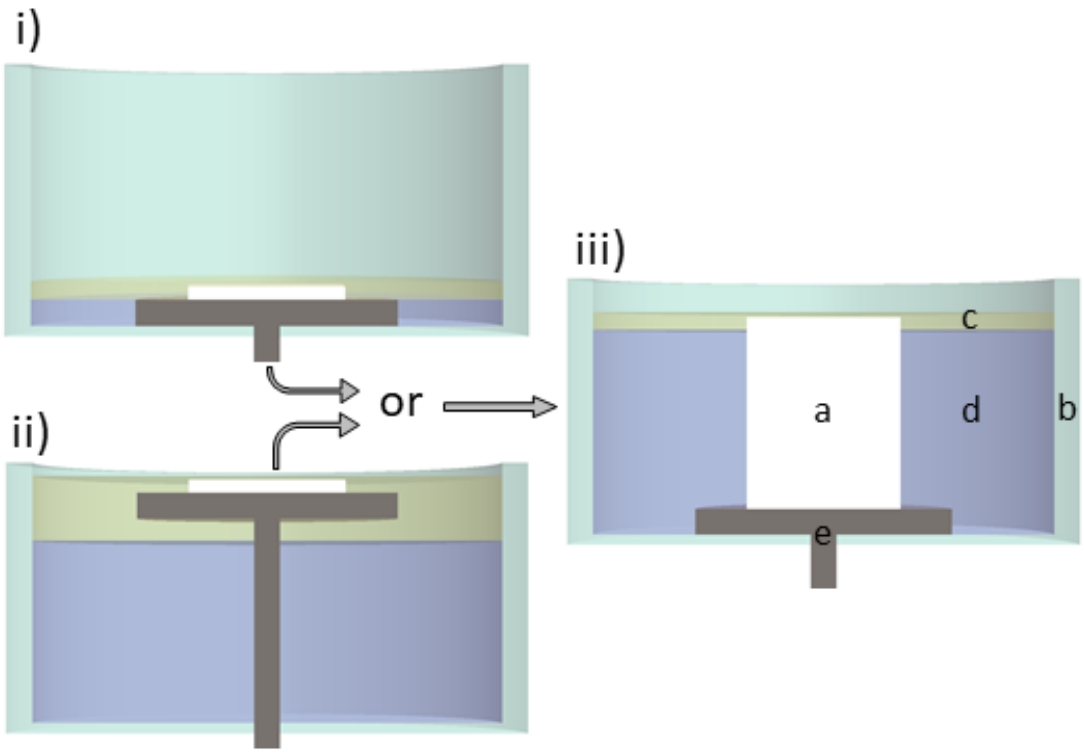

Figure 6: CAD visualization at two approaches to bottom-up printing at the liquid-liquid interface. In i), the build stage remains stationary while more subphase is pumped into the system to raise the level of the resin over the course of the print cycle. In ii), the build stage lowers in the traditional way except that reservoir is primarily filled with a liquid subphase instead of resin. Both i) and ii) will look like iii) at the end of the print where a) is the printed part, b) is the borosilicate reaction vessel, c) is the resin, d) is the subphase, and e) is the build stage.

Subphase Specific Considerations

The selection of an appropriate subphase is not a trivial endeavor and has been the focus of much of the author's research. While the resins used during this research were limited to 2 commercial acrylate based compositions, the subphases explored represented a greater chemical diversity and multiple factors were considered during the selection process. After testing saturated sodium chloride in water, saturated sucrose in water, saturated sodium chloride in water with 1 wt% lauryl glucoside as a

surfactant, saturated sodium chloride in water with 1 wt% Alconox detergent as a surfactant, ethylene glycol, corn syrup (yes, it transmits enough UV to cure the resin and is fabulously viscous and dense), and HFE-7200 (ethyl nonafluoroisobutyl ether); a perfect subphase was elusive and instead the problem was treated as an optimization based on a compilation of the properties.

UV Transmission

When using a top-down printing configuration, it is critically important that the subphase not significantly absorb or scatter UV light as that would reduce the energy available to the resin for curing and reduce the lateral resolution, respectively.

In this experimental setup, there are several materials to consider for absorbance. The projected image must pass through the borosilicate glass vessel, the liquid subphase, and into the liquid resin in order to cure the resin.

The irradiance incident to the resin is used in several calculations and so an attempt to experimentally measure it. An optical power meter (GaAsP photodiode, 370 nm peak response, ±5% ref NIST (NBS)) in a manner similar that described in Sun et. al.'s publication [60] was used to measure the incident irradiance at various distances from the source and passing through just air, through the reaction vessel, and through the reaction vessel and saturated salt water. The results of these measurements were inconclusive as the primary wavelength (405 nm) of the light source used (the DLP from Autodesk's Ember printer) is outside of the detector's range. A reading of 0.7 mW/cm^2 was measured for the range of 0-10 cm from the printer's surface and for any combination of air, reaction vessel, and salt water. Since another measurement technique was not available, the manufacturer reported irradiance of 20 mW/cm^2 was

used [76]. Good agreement is seen when comparing the experimental working curve for the Autodesk PR48 resin using 20 mW/cm^2 against the values reported by Bennet for 405 nm [102].

Absorbance data

The primary subphase classes were studied using a UV-Vis spectrometer to determine their absorbance behavior for the near UV range centered around the 405 nm excitation used by the DLP. The data is shown in Fig. 7, below.

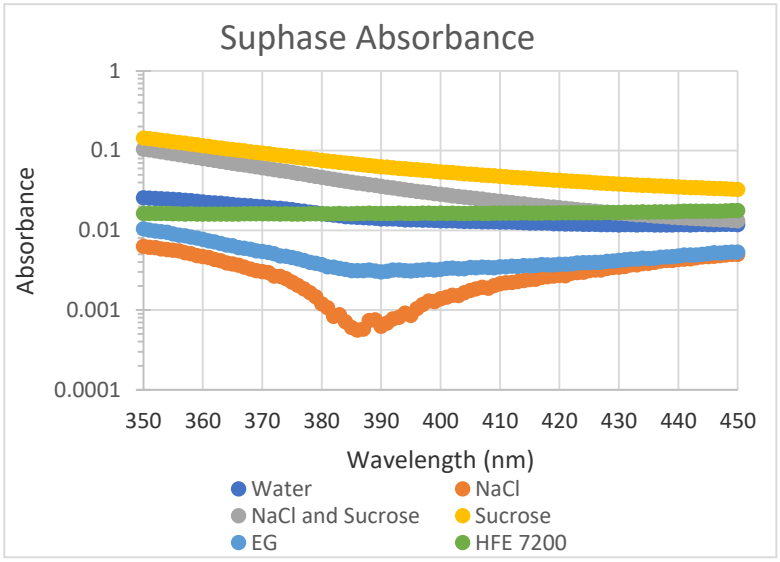

Figure 7: Absorbance of Subphases

The subphases studied were deionized (DI) water, saturated sodium chloride in DI water (referred to as salt water in this thesis), saturated sucrose in DI water, DI water saturated with both sodium chloride and sucrose, ethylene glycol (EG), and a hydrofluoroether (HFE) which is known by the trade name of 3M Novec HFE 7200 or

ethoxy-nonafluorobutane ($C_4F_9OC_2H_5$). While none of the subphases exhibited critically high absorbance in this range, the solutions containing sucrose had approximately 10 times more absorbance than the other aqueous solutions or the organic subphases.

Environmental Considerations ("Green-ness")

One of the factors that the author personally wanted to be a consideration in the subphase selection process was its environmental friendliness. Ideally, this work will identify a wildly successful way of printing that will be commercially successful and adopted around the world. If that happens, large volumes of the subphase will be transported, used, and become waste. The same is true of the resin but the resin has pre-defined chemistries that are necessary to its function and so this discussion is limited to the subphase selection. Both aqueous sodium chloride and sucrose are considered low-hazard both to human health and the environment. EG is poisonous to humans but is used extensively for airplane deicing without major incident. EG is known to biodegrade in soil, have a one day half-life in air, and decomposes both aerobically and anaerobically in water and so is viewed as posing "little threat to the environment" [103]. HFE 7200 is an inert fluorinated solvent. It is non-toxic but due to its high stability, has a 100 year global warming potential of 69 when compared to carbon dioxide [104].

Resin-Subphase Considerations

Many of the properties that determine if a subphase will perform as desired cannot be considered in isolation but must be thought of as complimenting the resin used.

Density

The density of the subphase must be greater than the density of the resin to facilitate layer separation. Both resins have a density greater than water which eliminated what would have been the cheapest, least hazardous, and most readily available potential subphase from consideration. It was experimentally verified that neither resin will float on water. Table 2 shows the densities of both resins and of the subphases. Some values come from the cited sources while others were determined experimentally.

Table 2: Subphase and resin densities at room temperature in g/mL. Values from literature are shown in parenthesis.

Autodesk Clear Prototyping Resin	MakerJuice G+ Resin	Saturated NaCl	Saturated Sucrose	Saturated NaCl and Sucrose	HFE 7200	Ethylene Glycol
1.13	1.13 (1.1 [105])	1.23 (1.202 [106])	1.29 (1.33 [107])	1.36	(1.43 [108])	(1.115 [109])

Some of the experimentally determined behaviors can be predicted from this table. For example, when trying to float either resin on EG, it is observed repeatedly but at random intervals that the resin will displace some of the EG and partially sink to the bottom so that there are two vertically parallel phases as shown in Figure 8, below. A possible reason for this phenomenon is that the surface energy is lowered in this configuration and that the buoyant forces are minimal as the densities are almost equivalent.

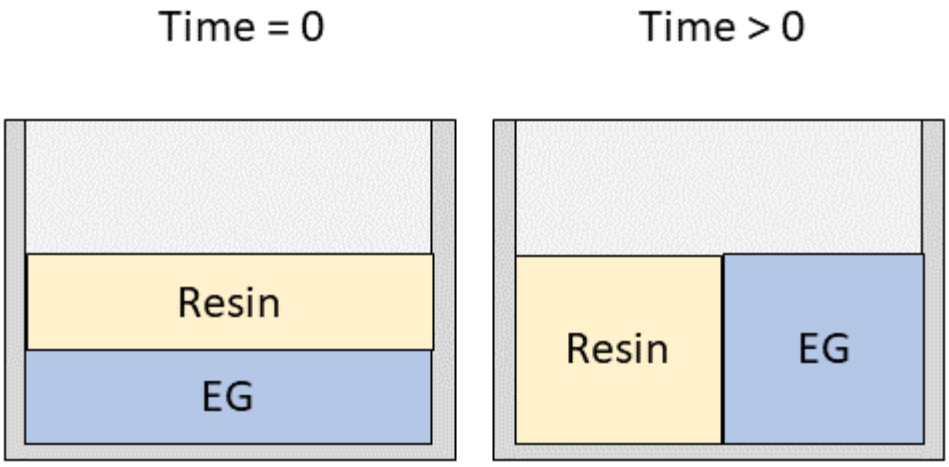

Figure 8: Observed behavior of resin dispensed over ethylene glycol. Note that eventual segregation into adjacent instead of parallel phases is due to a combination of the immiscibility, nearly identical densities, and a spreading coefficient less than zero (S<0).

Immiscibility

The resin and subphase must be immiscible so that they remain as two separate liquid phases. Immiscibility was studied by dispensing a known volume of subphase into a vial, marking the height, and then dispensing a known amount of resin on top of the subphase. It was observed if the volume of either the upper or lower phases changed. Next, the capped vial was a metered number of shakes and the resulting behavior was observed. With the exception of EG, all of the subphase-resin pairings separated to the original volumes when left to sit overnight. A summary of the mixing results and determination of degree of immiscibility can be found in Table 3, below.

Chemical Compatibility and Stability

The ideal resin-subphase pairing will be chemically stable for prolonged periods of exposure to each other. If the resin and subphase chemically react with each other this

would be unfavorable. In a best-case scenario, the resin could be left floating on the subphase and remain viable for printing after being left for week or month. A summary of experimental tests of sustained chemical compatibility can be found in Table 3, below.

Surface Tension, Wetting, and Spreading

Surface energy(γ) effects play a critical role in printing at the liquid-liquid interface. Surface energy, also known as surface tension, is a measurement of how energetically unfavorable it is for a molecule to be at the surface of a liquid instead of surrounded by other molecules in the bulk liquid. It is proportional to the intermolecular forces and inversely proportional to molecular size [110].

The degree to which the resin spreads across the subphase, known as wetting, is a function of the the surface energy of the air-resin-subphase interface, which is in turn a function of the surface tension of both the resin and subphase.

Antonoff's rule is commonly used to predict the spreading behavior of immiscible liquids via a simple comparison of the surface tensions as shown in Eqn. 15 [111].

$$\gamma_{AB} = \gamma_B - \gamma_A \qquad \textbf{Eqn. 15}$$

In the above equation, the interfacial tension (γ_{AB}) is difference in surface tension (γ) between the upper liquid A and lower liquid B. If γ_{AB} is greater than zero, the resin is expected to spread over the subphase according to Antonoff's rule. However, Antonoff's rule is not always reliable for systems with a highly polar subphase (like water) or for amphipathic organic liquids [112]. In those cases, Fowkes's correction can be used which adds a term to Antonoff's rule to account for the dispersion forces

from both nonpolar sources and hydrogen bonding. In the equation below, γ^d is the surface tension contribution of a pure liquid due to dispersion and is equal to γ for nonpolar liquids [111], [113]. γ^d can be determined experimentally or found in published tables for some liquids.

$$\gamma_{AB} = \gamma_B - \gamma_A - 2\sqrt{\gamma_A{}^d \gamma_B{}^d} \qquad \textbf{Eqn. 16}$$

Another important phenomenon is the spreading of a thick film due to gravity. The spreading coefficient (S) is useful to introduce. If S is greater than zero, the system is expected to wet. S can be written both as a function of surface tension and as a function of density, gravity, and a critical film thickness (t_c). This thickness is of the metastable state where the thinnest possible layer of resin has been spread over the subphase and any disturbance would cause it to de-wet [110].

A final surface energy effect that is critically important to this approach to SL is capillary action. Before the first projection when there is only liquid resin and there is a true liquid-liquid interface with no capillary action if one considers only the center of a wide bath. However, as soon as the first layer of resin cures, there is now a liquid-liquid-solid interface and, dependent on the surface energy of each, a meniscus can for either into the subphase or, more commonly, into the resin. The height of this meniscus scales with the surface tension divided by gravity and the effective density to the half power. De Gennes's book [110] on the subject is highly recommended but, to summarize, 1) the capillary height of the subphase rising into the resin can be even higher than in air due to the buoyant forces from the displaced resin, 2) since the capillary height is inversely proportional to the effective density, a high density

subphase and low density resin will produce the smallest height, and 3) a lower surface energy subphase will have a shorter capillary height.

When the subphase's capillary effects wet or wick onto the printed part, the subphase can displace the liquid resin from the print interface. This can cause voids in the print as the build stage may be raised for several layers before the capillary height is exceeded and gravitational forces overcome surface energy effects and restore a liquid-liquid interface. In some cases, this can cause complete print failure as the exposure time may be insufficient for the resin to cure and bridge a multi-layer gap.

While this work is primarily focused on the speed of printing, other applications require a monolayer for achieving the thinnest possible cured layer height. When a small volume of resin is pipetted onto any of the subphases tested, individual beads or pools form instead of wetting the liquid-liquid interface to form a monolayer. The tightness, or diameter to volume ratio, of the beads is a function of the subphase's surface tension and phobicity to the resin. Ethylene glycol had the loosest resin beads for small amounts of resin while HFE had the tightest. On certain resin-subphase pairings, a sheen similar to a transparent oil drop spread over water was observed even though the majority of the resin remained in a beaded drop.

Many printing experiments were performed using a thick (1+ cm in height) resin layer to force the resin to form a continuous layer and to take advantage of the gravitational pressure head to assist in replacement resin inflow after a layer has been cured and displaced.

Resin Spreading

One of the factors that can potentially limit the print speed of a multi-layered part is the velocity of the resin spreading. If the volume of resin being cured into a solid and lifted with each layer is greater than the volumetric flow of resin to replace it, the print will have voids and possibly fail to print later layers. Due to the rapid print rate desired, the spreading velocity of the resin due to surface forces is insufficient to replace the cured volume. Instead of using a thin layer of resin that spreads due to interfacial tension alone, this research used a thick layer of resin so that the pressure head from gravity assists in the spreading as described in the next section. The time required for a film to spread is known to scale with the distance (d) as $d^{4/3}$ [114]. It is therefore advantageous to print narrow cross sections, like are present in a gyroid, when trying to achieve maximum print speed.

Subphase Entrainment

When printing a multi-layer object, dynamic characteristics of the subphase come into play. If the subphase has a surface tension greater than that of the resin, it will preferentially wet solid surfaces. This can be observed in the shape of the meniscus at the edge of the print vessel. While there are initially no solid surfaces to wet in the middle of the liquid-liquid bath, as soon as the first layer cures a solid is present. The subphase can preferentially wet the cured part as is it raised from the interface and temporarily displace the resin below the cured layer as shown in . Eventually the part will raise high enough that gravitational forces will overcome the interfacial tension forces and the subphase will rebound into a flat interface. However, there may be one or more layers during which no resin was cured if the part has a constant cross section

as the subphase displaces resin below the previous layer. This creates large voids in the printed part and has caused multiple repeated print failures during this research.

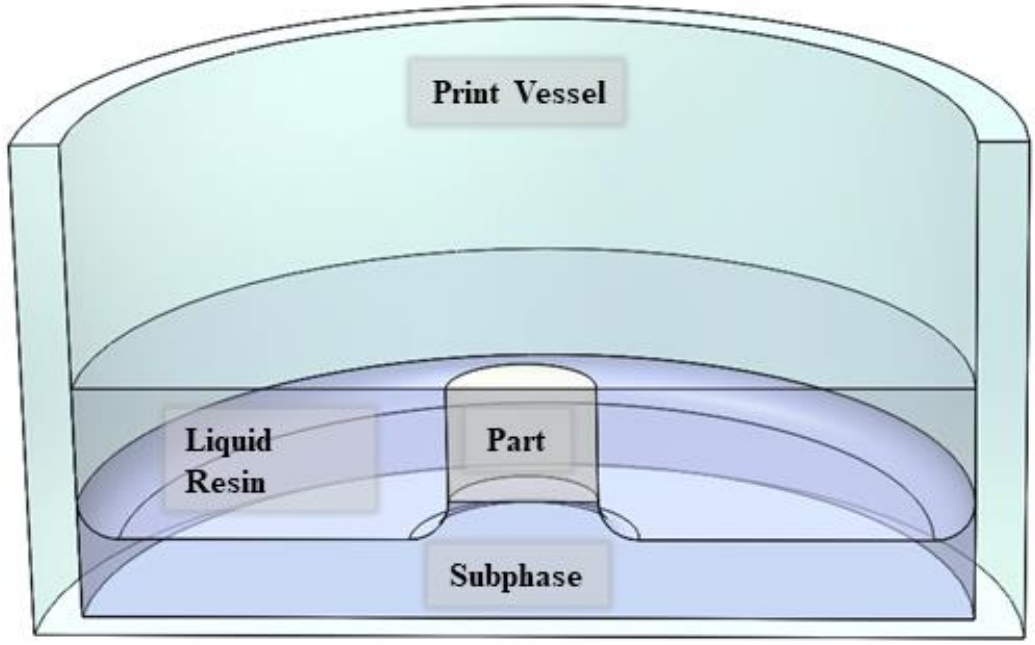

Figure 9: Cross section showing the subphase displacing the resin at the interface by wetting the solid part. (Build stage not shown)

There are several ideas about how to solve the problem of entraining subphase liquid in the printed part including i) reduce the surface tension of the subphase (easier than increasing the surface tension of the resin), ii) print objects similar to a 3D checker board so that there is minimal overlap between successively cured layers, iii) increase the height of the standing resin pool to increase its gravitational pressure, and iv) increase the layer height for maximum vertical displacement between each cross section so that the gravitational force from the liquid resin has the best chance of exceeding the interfacial forces even though this will reduce the vertical resolution.

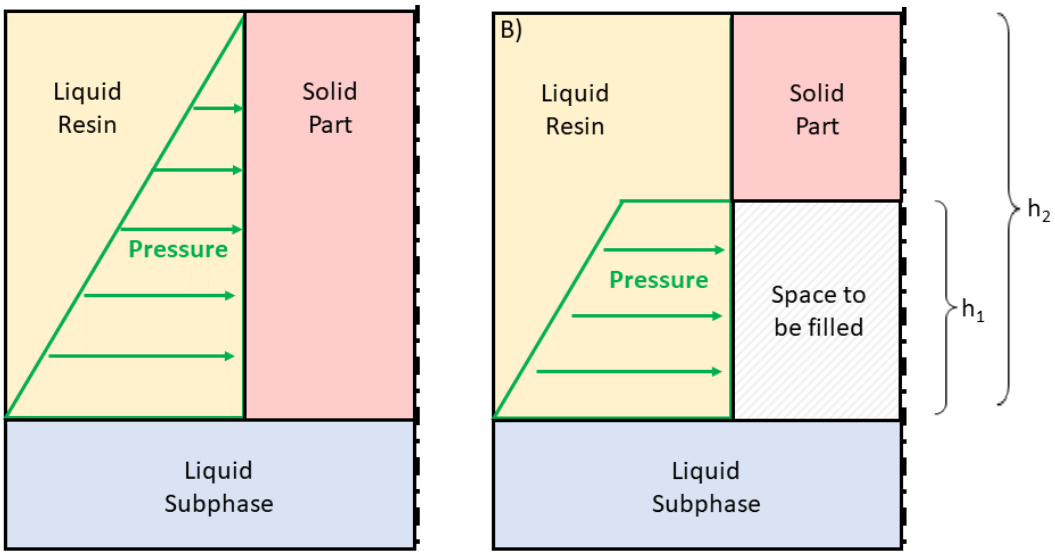

Figure 10: Pressure and force due to gravity. A) illustrates the pressure distribution changes over depth while B) shows the space made available by lifting the cured layer. This space can be filled with resin and/or subphase and is the area over which the force acts. The dashed line represents the center over which the system is symmetric.

A good approximation of the magnitude of the pressure and forces due to gravity at the resin-subphase-cured part liquid-liquid-solid interface can be achieved using a condensed version of Bernoulli's equation (assume that at t=0 there is no flow, no other elevation effects). The case for the pressure acting over the entire height of the resin on the solid cured part is shown from part A of the figure above in . This relationship between the resin's density (ρ), acceleration of gravity (g), and total height of the resin (z) gives the pressure exerted over the surface of the cured resin. The portion of the pressure that will act on the liquid that fills the empty space created by raising the solid part at time zero is shown as P_B. The force that this portion of pressure exerts on the liquid at time zero is a function of P_B, the liquid height (h_1), and the constant perimeter of the printed part (C).

$$P_A = \rho g z = {}^1/_2 \rho g h_2 \qquad \textbf{Eqn. 17}$$

$$P_B = \rho g (h_1 h_2 - \frac{{h_1}^2}{2}) \qquad \textbf{Eqn. 18}$$

$$F_B = P_B h_1 C \qquad \textbf{Eqn. 19}$$

In order for the resin to spread into the empty space instead of the subphase being sucked in to fill it, the force from the resin's gravitational head (F_B) must exceed any interfacial forces like capillary effects that oppose resin spreading. This supports the experimental observation that the resin displaces the subphase under the printed layer as h_1 becomes large.

Subphase Selection Summary (Static)

A summary of the static (vs dynamic print) properties and behaviors of the subphases is presented below in Table 3.

Table 3: Summary of the subphase performances on multiple selection criteria.

	HFE	Ethylene Glycol	Saturated NaCl (aq)	Surface Tension Modified NaCl(aq)	Saturated Sucrose (aq)
UV Transmittance	3 Average	4 Above average	5 Best	4 Above average	2 Worst
Environmental Score	3 Acts as a green house gas	3 Poisonous	5 Benign	5 Benign	5 Benign
Immiscibility	5	2	5	4	5

	Excellent, repels resin	Slight miscibility	Excellent	Good	Excellent
Spreading	1 Resin forms tight droplets	3 Sheen forms, droplets	2 Slight sheen forms	3 Sheen forms, droplets	2 Slight sheen forms
Stability	2 Becomes opaque overnight	1 Resin separates and partially cures overnight	5 Excellent, can print after a month	3 Good, can print after a week	4 Good, can print after a week

From this analysis, the saturated NaCl solution and surface tension modified saturated NaCl solution are the best candidates for the subphase.

Resin Impact on Print Speed

The importance of resin cure speed will soon be shown. While other steps may more severely limit the system's print speed, the resin curing rate sets the theoretical maximum print speed that is possible. This speed is found through the analysis of the working curve which is traditionally presented as thickness vs dosage [49], [93], [115], [102]. The benefit of this presentation method is that it allows comparison of a resin's behavior independent of the light source's intensity. The plots comparing speed and thickness vs time, which are source specific, are included for reference in APPENDIX 2 while the traditional format is presented in , below.

Working Curve

The working curve is an experimental way to find the maximum height of resin that can be cured per unit time for a specific resin and light source. When the working curve is displayed as cured depth vs time as is shown in in the Appendix, the instantaneous print speed can be found as the slope of the curve at any given time. As

is expected for the derivative of a logarithmic function, the print speed (μm/s) is proportional to the inverse of time (t).

$$C_d = D_p \ln(\frac{E}{E_{crit}}) \quad \textbf{Eqn. 20}$$

Equation of a line $y = mx + b$

$$\frac{d}{dt}[m \ln(t) + b] = {}^{m}/_{t} \quad \textbf{Eqn. 21}$$

There is some noise in the experimental data at the small times that produce the greatest print speeds as this approaches the critical exposure below which the resin will not cure. There may also be a time constant associated with the DLP's DMD orientating the micromirrors to reflect the projection. Additionally, any localized variations in the concentration of monomer or photoinitiator will result in significant differences in the cured thickness for very short exposures. For greatly improved repeatability at the sacrifice of a little print speed, it is recommended that exposure times less than 1 second not be used.

Working Curves at the Liquid-Solid Interface

The following working curves for the two commercial resins were found at a solid-liquid interface by adding resin to the top of a glass slide and projecting through the bottom of the slide. This method has been used in all of the literature studied, including the CLIP *Science* paper [49]. The exposure was found by controlling the projection time and applying a known irradiance (see previous experimental section).

Working Curves at the Liquid-Liquid Interface

The following working curves were made from measurements of films cured at the resin-subphase liquid-liquid interface. These are the first known working curves to be made for behavior at a liquid-liquid interface. Notice the many similarities between the working curves shown in . The data closely match each other in distribution, slope, and intercept. However, the data for the liquid-solid curve has measurements from films both thicker and thinner than what is reported at the liquid-liquid interface. This is due to the challenges of printing at a floating interface. While films as thin as those measured at low exposures in the liquid-solid experiments are visually observed to form during liquid-liquid experiments, they are exceedingly difficult to recover and measure. These fragile films are free floating in a liquid and must be recovered with tweezers or the scientific analog of a slotted spoon (see in in the Appendix) and, once recovered, must be strong enough to survive handling and measurement. Films below a threshold thickness are too delicate to recover and to measure without the benefit of a rigid, solid substrate. The most common failure modes for these thin films is folding and adhering to itself or ripping. Films that are too thick are also problematic when floating at the liquid-liquid interface. Cured resin is more dense than liquid resin and, if the cured layer is heavy enough, can cause distortion of the interface. The weight of thick layers pushes the interface down in the middle of the reaction vessel and up near the edges, causing a bow shape. This bowing, coupled with the stresses from the shrinkage as it cures from liquid to solid, results in a curved or curled part. This shape deformation gets worse as the layer thickness increases and, especially when using the fast curing MakerJuice resin, it has been observed that the part will curl so severely

during the projection that the edges will break the resin's top surface while the middle sags into the subphase resulting in unintended separate layers near the edge. The visual effect is similar to setting an open hardbacked book down while it is open. A flat, continuous part is needed for measuring the thickness and so thick films from the free liquid-liquid interface cannot be used.

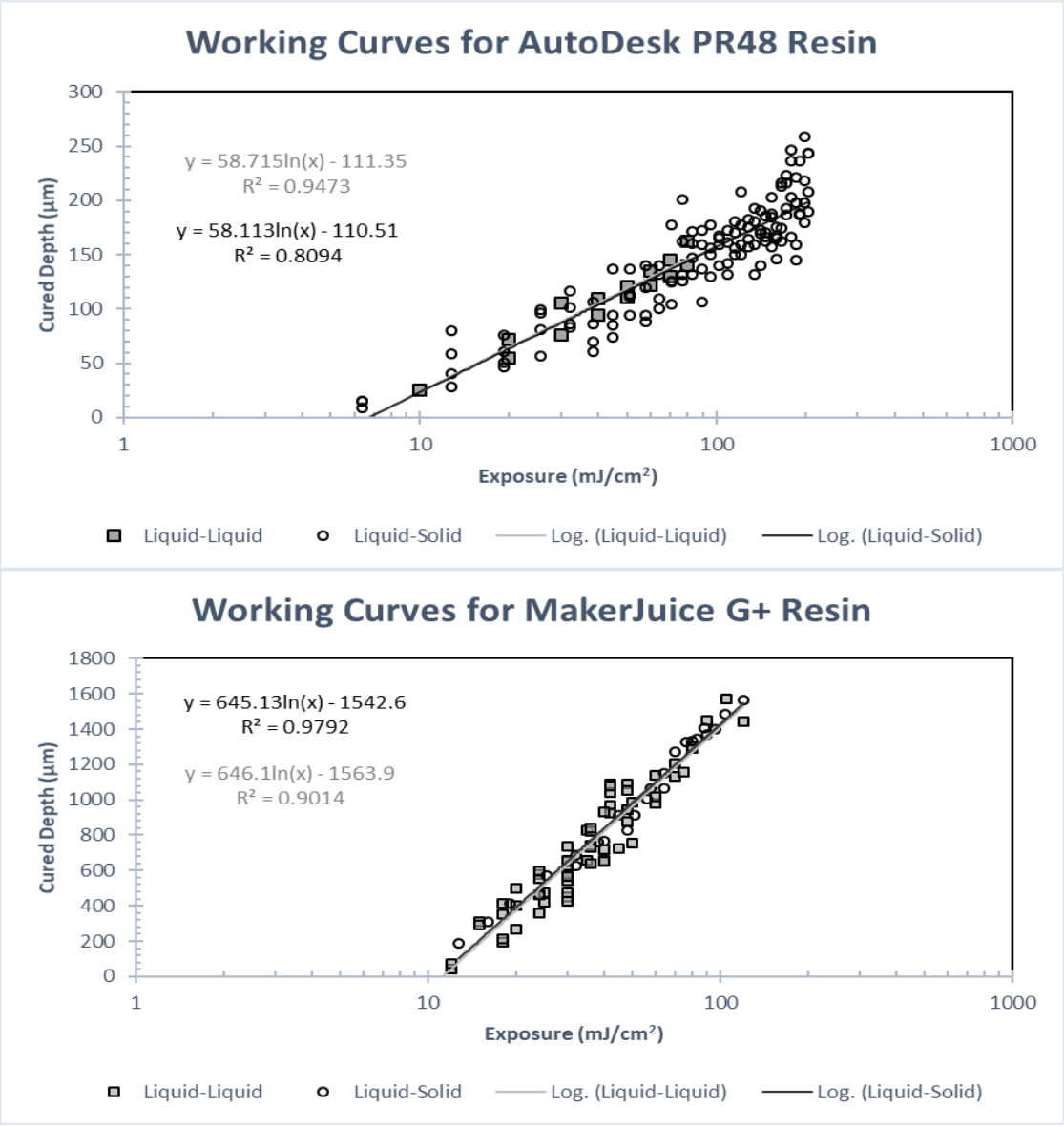

Figure 11: Working curves for Autodesk's Clear Resin (PR48) and MakerJuice's G+ Resin grown at both the liquid-solid and liquid-liquid interface.

Maximum Resin Print Speed

In less than a single second of light exposure, the Autodesk resin reaches its maximum print speed of 91 µm/s which is equivalent to 33 cm/hr (see the alternate forms of the working curves presented in APPENDIX 4). The MakerJuice resin has a higher E_{crit} but also has a large minimum layer thickness and can cure at rates exceeding 450 µm/s or an impressive 162 cm/hr.

Comparison to Other SL Methods

How fast is 162 cm/hr? It is 90 times faster than the Ember printer which can print 1.8 cm/hr [68]. It is also more than three times as fast as the 50 cm/hr made possible by the CLIP process [49]. While this speed is exciting, there are some considerations that must be taken into account when trying to realize this speed in a fully 3-dimensional part printed at the liquid-liquid interface.

Speed Limiting Steps of SL

There are several steps within the SL cycle that can limit print speed. While some of these limits are the same across all systems, many are unique to the print method used.

Traditional SL Speed Limits

Traditional SL here refers to techniques that require a delamination step. The main steps of this technique are shown below in Figure 12. In the first pane, the liquid resin is polymerized by the incoming UV light. The polymerization progresses such that the liquid cures and connects this new layer to both the prior layer and to the bottom of the print vessel. While connecting to the previous layer is desired, the new layer must be delaminated from the print vessel. This delamination step takes time. Over the years,

many clever methods like rotating the print vessel, pivoting the print vessel, or even using a flexible print window, in addition to the obvious vertical pull have been developed. All of the delamination methods require the polymerization to be stopped and limit the overall print speed.

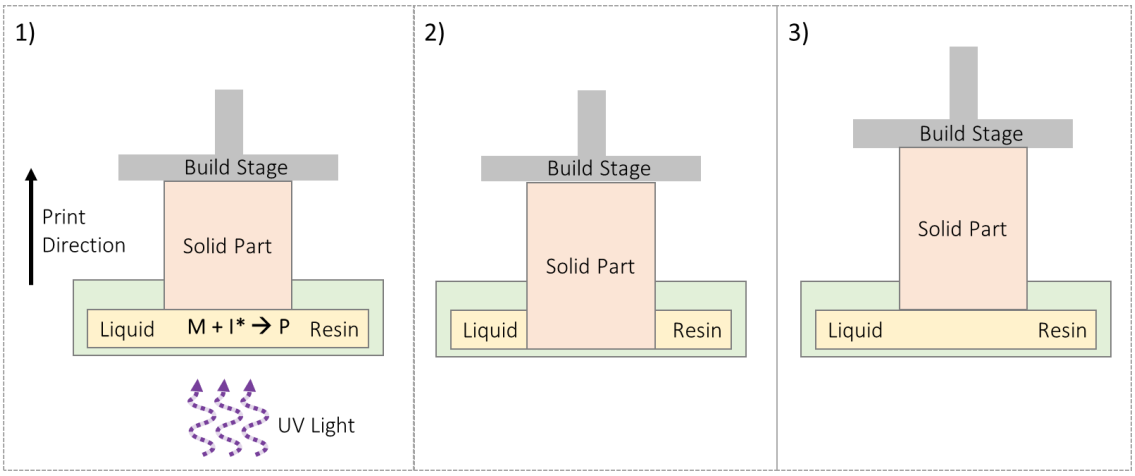

Figure 12: Printing Steps for Traditional SL Techniques. During 1 the liquid resin is cured to a solid in the pattern of the incident UV light. After the layer is polymerized (2), the new layer adheres both to the printed part and to the print vessel. In 3, the solid part has been separated from the print vessel and lifted so that it is ready to repeat step 1.

In addition to the delamination step, the speed of moving the build can limit the speed of traditional SL. Some delamination techniques incorporate the raising of the build head but others require it to be lifted as a discrete step before the next layer can be projected and cured. The speed of the motor or other mechanical displacement method can further reduce the system's print speed.

The other fundamental limit to SL print speed is the progression of the photopolymerization reaction. It takes time for a photon to be absorbed by a photoinitiator, for the PI to activate, and for the activated PI to link monomers together. While this was discussed in detail above, it is worth repeating and noting that

different resin chemistries have different reaction rates and the print speed could almost certainly be increased beyond what is reported here using two commercial resins. An ideal resin for an application only requiring speed would have no UV blocker, a minimal amount of PI, a low viscosity to aid spreading, and no oxygen inhibition. This configuration (no UV blocker, low PI concentration), allows for the curing of thick layers that are necessary for very fast printing. In this case, print speed is achieved at the expense of resolution. The speed is further dependent on the size and degree of crosslinking of the monomer. Much like the various sizes of children's building blocks, it is faster to build with larger components that require fewer pieces to be assembled to form the desired height. The print speed of the two resins tested can be found from the working curves presented in APPENDIX 2 and the system speeds of various SL-based printers in APPENDIX 3.

The difference between the system printing speed and the resin curing speed is about an order of magnitude. 1.8 cm/hr [68]is an average print speed for printers using a traditional SL technique while the fastest reported is to 6.0 cm/hr [116]. The Autodesk PR48 resin's maximum print speed is 91 cm/hr and the MakerJuice G+ resin's is 162 cm/hr. The difference between the resin print speed and the system print speed for a traditional SL system can be attributed to the delamination step and mechanical displacement.

CLIP Speed Limits

The CLIP method of SL, as presented in the 2015 *Science* article [49], is able to achieve a faster print speed than traditional techniques by eliminating the need to

delaminate each printed layer. Their unique setup (Figure 13) improves the system print speed but also introduces a new limiting phenomenon. CLIP relies on the diffusion of oxygen from the air or an oxygen enriched environment through a permeable glass to inhibit the photopolymerization reaction near the glass. As was previously discussed, the oxygen competes with the resin polymerization reaction by removing the photoexcited photoinitiators' free radicals from the system. When the concentration of oxygen dissolved in the resin is high enough, as is usually the case immediately about the permeable glass, it prevents the polymerization reaction from proceeding. The area where the oxygen concentration is high enough to inhibit polymerization is referred to as the dead zone. The height of the dead zone is dynamically dependent on the concentration gradient of oxygen across the permeable glass and by the print speed [49]. As the print speed increases, the concentration of oxygen is depleted due to the inflow of fresh resin and the dead zone height decreases. At high print speeds, the resin flow can also cause instability of the dead zone and this is the phenomenon attributed with limiting the print speed [49].

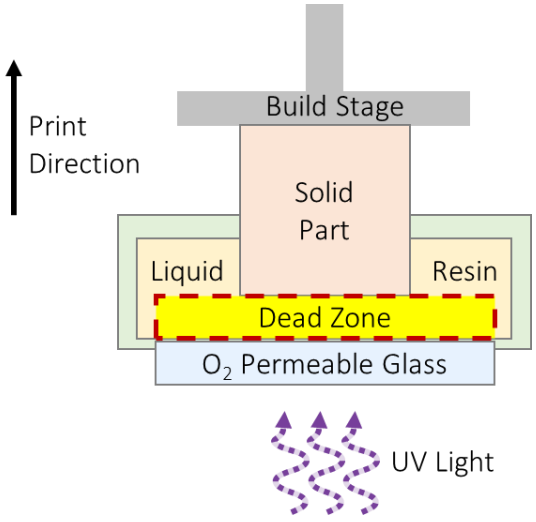

Figure 13: Schematic of the experimental setup of the CLIP technique

CANFI Speed Limits

The CANFI approach to SL is similar to the CLIP method in that it too eliminates the need to delaminate each printed layer. CANFI achieves this by using a liquid subphase below the resin and above the glass of the print vessel. By using a liquid subphase instead of an oxygen permeable glass, CANFI can improve print speed both by eliminating the reliance on oxygen diffusion and by reducing the interfacial instability by printing at a liquid-liquid interface instead of at a liquid-solid interface. Due to this unique setup, CANFI's Speed limits are different than both traditional SL and CLIP. CANFI's maximum theoretical print speed limit is the curing speed of the resin while, in practice, the speed tends to be limited by the interfacial effects between the resin and subphase. If the resolution and print quality are not considered, then print speeds approaching the resin's theoretical maximum have been experimentally demonstrated using the CANFI method. The current prototype printer consists of a hacked Ember printer from Autodesk and is not capable of truly continuous printing as there is an interlock that does not allow the UV DLP to be on while the vertical stage is moving. This means that all prints were generated using a semi-stepwise print method consisting of resin exposure and then lifting the layer. This caused slower system print speeds than the CANFI method should be capable of as the time between the DLP's shuttering, the raising of the build stage, and the re-initiation of the DLP is wasted. Despite that, system print speeds of 81 cm/hr were demonstrated using the MakerJuice G+ resin printing 0.9 mm layers for every 2.1 s of exposure. This corresponds to a 3-dimensional resin print speed of 159 cm/hr if only the time the DLP is on is counted, which is reasonable as the next prototype should be capable of this continuous

projection and displacement. These speeds are remarkable as the non-continuous prototype's speed is about 50% faster than CLIP and the resin has been demonstrated to be capable of 3-dimeninsionally replicating its theoretical maximum speed from the 2-dimensional working curve.

It is important to treat these findings as proofs of concept and not as the values from a completely finished design. While these print speeds are impressive, they come at the expense of vertical resolution as, currently, large layer heights are needed to take advantage of the fastest resin curing regimes. Furthermore, the dynamics of the resin-subphase and resin-subphase-solid part interfaces are a new system of study and an ideal pairing of resin and subphase has yet to be identified. Prints using the low surface energy and high density HFE-7200 as a subphase produce good feature resolution at lower print speeds but high speed prints have not been achieved and there is a side reaction that occurs between the HFE and the resin. This side reaction does not inhibit printing but does cause the printed part to appear opaque (like white clouds) and is thought to be due to oxygen dissolved in the HFE. Printing on saturated salt water typically produces poor quality parts as the salt water's high surface energy allows it to preferentially wet the printed layer and displace resin from the interface, thereby inhibiting one or more layers from printing until the part is eventually raised high enough that gravitational forces overcome surface energy effects. However, the fastest 3D print speeds were achieved on salt water.

Printing Fully Three-Dimensional Objects

While beautiful, thin, free-floating films can be readily printed at the liquid-liquid interface (see photos in APPENDIX 4), fully 3D objects are more challenging. In the table below, the quality of a printed object was ranked from 1 to 5 for both resins using different printing parameters, layer heights, and subphases. Please see the parameter and print result keys at the bottom of the table for details and note that the maximum layer height used for the Autodesk resin is less than that used for the MakerJuice resin due to a difference in C_d.

Table 4: Summary of results from 3D printing at the liquid-liquid interface.

MakerJuice G+ 3D Printing Results					
		I	II	III	IV
Subphase	Step size (μm)	Plain	Wait	Overlift	W+O.L.
Saturated NaCl(aq)	10	F			
	50	D	C	C	B
	500	D			
Surf. Ten. Mod. Sat. NaCl	10	F			
	50	D	C	C	B
	500	C			
HFE-7200	10	C			
	50	B	A	B	A
	500	B			
Autodesk PR48 Resin 3D Printing Results					
		I	II	III	IV
Subphase	Step size (μm)	Plain	Wait	Overlift	W+O.L.
Saturated NaCl(aq)	10	F			
	50	D	C	C	C
	100	D			
Surf. Ten. Mod. Sat. NaCl	10	F			
	50	D	C	C	B
	100	C			
HFE-7200	10	C			
	50	B	B	B	A

	100	B			
Print Results Key					
A	More than 90% of the layers formed as expected, good dimensional agreement with CAD model				
B	Object about the expected size and shape but some layer damage				
C	About half of the object printed as expected, resembles model				
D	Entire height printed but part is unrecognizable when compared to model				
F	Less than half of the object printed as expected				
Print parameters Key					
I	Exposed for time predicted by working curve +10%				
II	Exposed for time predicted by working curve +10%, waited 1 s before projecting the next cross section				
III	Exposed for time predicted by working curve +10%, lifted the build stage an extra 50 um before lowering it to the printing height between every cross section projection				
IV	Exposed for time predicted by working curve +10%, both lifted the build head an extra 50 um and waited 1 s before projecting the next cross section				

From these results, it can be concluded that print quality at a liquid-liquid interface generally improves as the layer height increases, as a wait time or over-lift are added, and as the subphase surface tension of the subphase decreases. The average print quality for each subphase is shown below in Table 5. Note that print quality generally increases as density increases and surface energy decreases.

Table 5: Summary of Subphase's Density and Surface Energy vs Print Quality

	HFE-7200 [1]	Ethylene Glycol [2]	Saturated $NaCl_{(aq)}$ [3]	Lauryl Glucoside in $NaCl_{(aq)}$ [3]
Density (g/cc)	1.43	1.11	1.21	1.21
Surface Energy (mJ/m^2)	13.6	47.7	82.5	~45

CHAPTER 4

CONCLUSIONS AND FUTURES

Conclusions

This work rederived the working curve equation for curing resin due to light and showed good agreement between this model and the resin behavior at a liquid-solid interface. Additionally, the first ever working curves generated at a liquid-liquid interface were presented and they closely match those from the liquid-solid interface. The current prototype printer has achieved 3D system print speeds of 81 cm/hr and demonstrated 3D resin curing speeds of within 2% of the maximum theoretical limit established by the 2D working curve. Efforts were made to increase the print quality of parts printed using the CANFI method at the liquid-liquid interface and high density, low surface energy subphases were identified as optimal.

Recommendations for Future Work

While the results of this research are exciting, there will always be a desire to push the envelope of what is possible with regards to print speed. Below are some recommendations for future work that are likely to yield even faster speeds.

Improved Hardware

Perhaps the easiest means of increasing print speed at a liquid-liquid interface, at least from a student's perspective, is to buy new equipment. The current prototype printer is not capable of truly continuous printing as the DLP cannot be operated while the build

stage is being moved. A fully programable integrated projector and motor would allow for truly continuous printing and eliminate the time wasted between projections while the motor moves up a step during which no printing occurs. Additionally, a higher intensity light source would reduce the time needed to cure a given thickness of resin.

Resin Formulations

There is the potential to harvest "low hanging fruit" by experimenting with the resin chemistry. Changing the type of chemicals in the resin has the potential to increase the reaction rate, lower the E_{crit} needed to solidify the resin, and increase the maximum cured thickness of a single layer. Both resins in this study were methacrylate based. There is at least one report of improving print speed by decreasing the concentration of PI [68]. To achieve maximum print speed, thick layers need to be printed which can be aided by decreasing the resin's specific absorption through the reduction of PI concentration.

Temperature

Reaction Rate

Chemical reaction rates are expected to be improved by heating the resin. Reaction kinetics typically scale strongly with temperature such that even a 10°C change can dramatically increase reaction rate. A journal article from 2018 has demonstrated preliminary findings on the accelerated curing of heated resins [115].

Print Quality

Viscosity and surface tension both decrease as temperature increases. A subphase with low surface tension is desirable to prevent preferential wetting, or wicking, onto the

printed layer. A low viscosity resin is also desirable as it will spread more readily. By increasing the temperature of the resin and subphase, it possible that both the part quality and printing speed will increase.

Subphases

The potential for success of printing at a liquid-liquid interface will always be tightly coupled to the resin-subphase pairing. This work tested a variety of materials as subphases including a polar aqueous solution, a nonpolar aqueous solution, an inert fluorinated organic, a polar aqueous solution containing an emulsifying surfactant, an organic compound commonly used as a subphase for the formation of nanoparticle monolayers, and even an organic based high density and high viscosity (di)saccharide polymer (corn syrup). Despite the diversity of materials tested as subphases, further work in this area is needed to achieve print quality that is comparable to slower, conventional SL methods.

APPENDIX 1

Terminology for Incident Light

Table 6: Disambiguation of Light Terminology

Absorption Coefficient	α	cm^{-1}	Absorptivity at a given wavelength
Absorbed Dosage	D	$\#/cm^2$ @given depth	Absorbed photon dosage per unit depth $D= \alpha\Phi_0 t \exp(-\alpha z)$
Absorption	A	$\#/cm^2$ s @given depth	Number of photons that are absorbed per unit area, time, and depth $A= \alpha\Phi_0 \exp(-\alpha z)$
Critical Exposure	E_{crit}	mJ/cm^2	Gel point, no curing below E_{crit}
Energy	e	J	Assume all photons have same wavelength so $e=hc/\lambda$
Exposure or Fluence	E	mJ/cm^2	Time interval of flux, "synonymous with dosage," light energy available to the system
Flux	Φ	$\#/cm^2$ s	Quantity of photons per unit area and time
Irradiance or Intensity	H	mW/cm^2	Radiant flux/power received per area

Exposure (E) is a measure of the amount of light energy available to the system. It has the units of energy per unit area and is most commonly measured in mJ/cm^2 [93]. Photopolymer resins remain liquid below a critical exposure (E_{crit}). The 'gel point' marks the resin's irreversible transition from the liquid phase to the solid phase, a phenomena not observed below E_{crit} [93].

The terms exposure (E), irradiance (H), dosage (D), and flux (Φ) are interrelated. While E is a measure of the available energy per area, H is a measure of the radiant

flux or power per area (e.g. mW/cm^2). As might be expected, exposure and irradiance can be related by the expression

$$E = \int \mathrm{H}\ dt\ . \qquad \textbf{Eqn. 22.}$$

Flux is simply the number of photons passing through a unit area in a unit time (e.g. #/cm^2 s). To find flux from an experimentally measured exposure, it is necessary to know the wavelength of the photons and helpful to assume a single wavelength is present. In the case of this research, a 405 nm LED light source was used [76]. For a nominal 1 mW/cm^2 irradiance, this would correspond to a flux of 2.04x10^{18} photons per cm^2 per s as shown in Eqn. 23 and Eqn. 24.

$$e = \frac{hc}{\lambda} = \frac{\left(6.626 \times 10^{-34} {}^{J}/_{s}\right)\left(2.998 \times 10^{8}\ {}^{m}/_{s}\right)}{405 \times 10^{-9} m} = 4.90 \times 10^{-19} {}^{J}/_{photon}$$

Eqn. 23

$$\Phi = \frac{E}{et} = \frac{H}{e} = \frac{1\ {}^{mW}/_{cm^2}}{4.90 \times 10^{-19} {}^{J}/_{photon}} = 2.04 \times 10^{15}\ {}^{photons}/_{cm^2 s}$$

Eqn. 24

Here the energy of a photon (e) is shown to be dependent on a relationship between its wavelength (λ), Planck's constant (h), and the speed of light (c).

Note: D refers to doseage while D_p represents the penetration depth of light. This terminology is found in the literature [49].

APPENDIX 2

Additional Working Curves

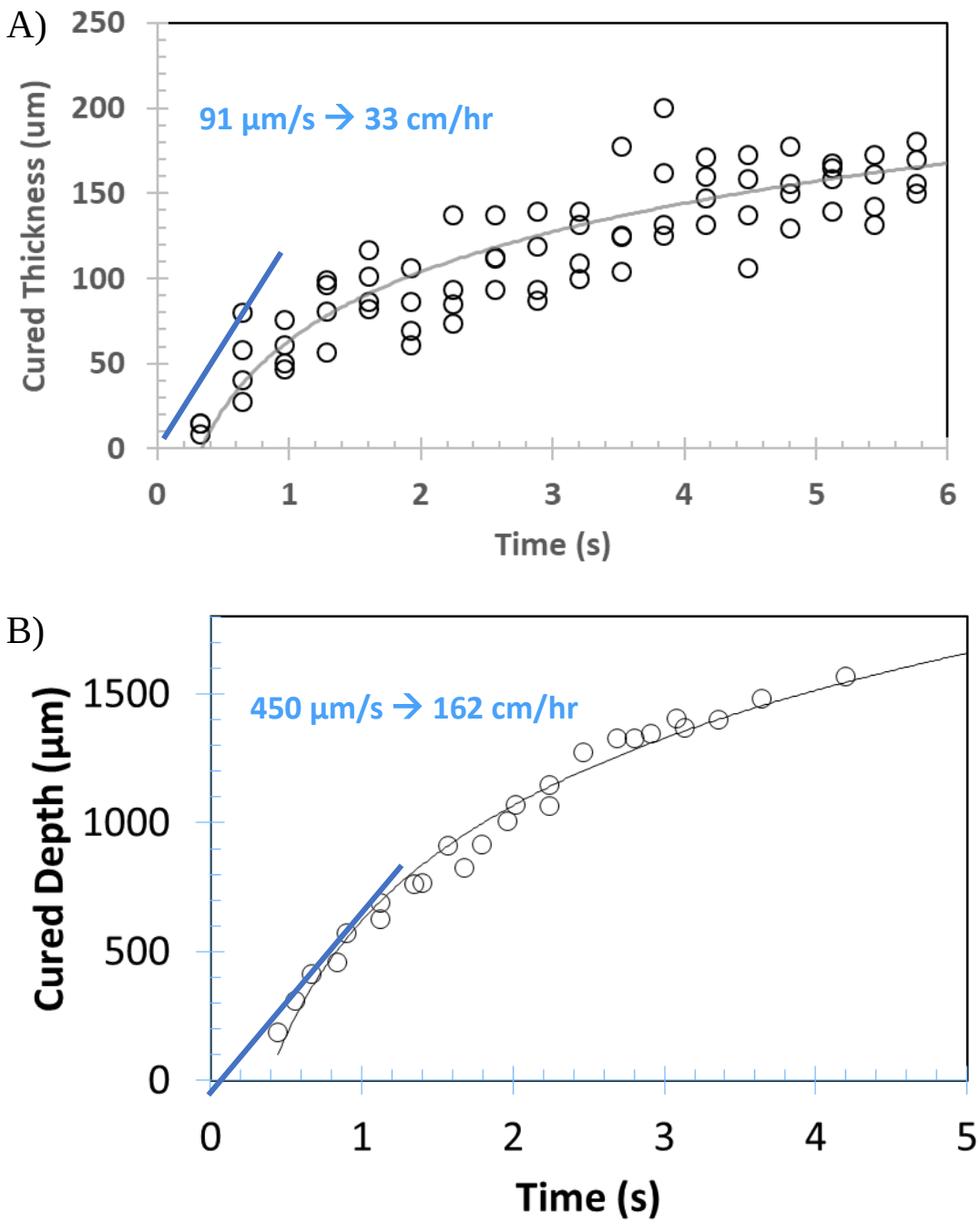

Figure 14: Working curves showing cured thickness vs time for a) Autodesk PR48 resin and b) MakerJuice G+ resin

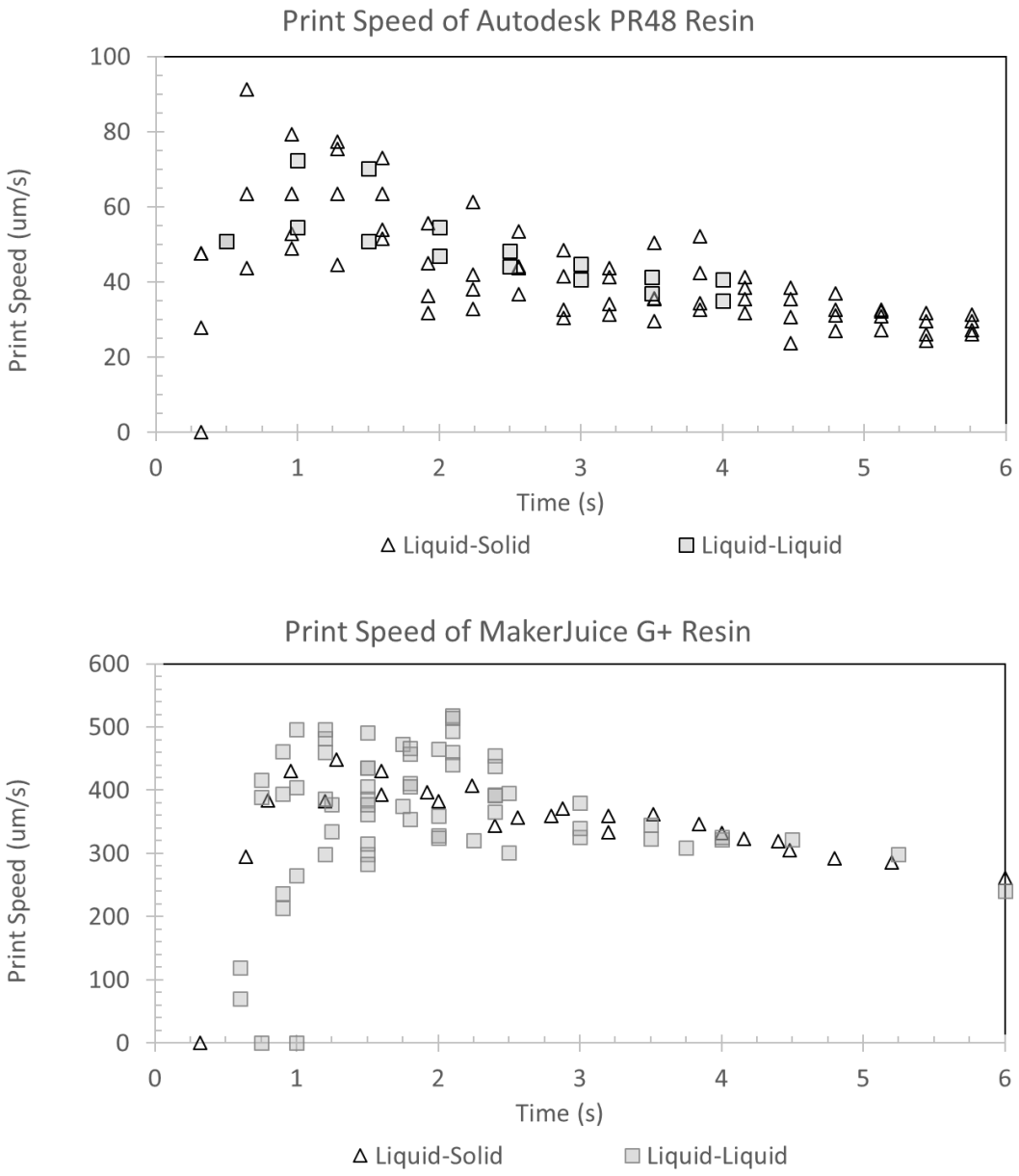

Figure 15: Comparison of the Print Speed of Two Commercial SL Resins at both the liquid-solid and liquid-liquid interfaces

APPENDIX 3

Speed of 3D Printers

Table 7: Print Speed of Other SL Printers

Printer	Print Technique	Speed (cm/hr)
Ember [68]	Traditional	1.8
G Printer [116]	Traditional	6
Ember [68]	Semi-continuous, high-speed configuration	44
Carbon[49]	CLIP method	50

Table 8: Experimentally Determine Print Speeds Using the CANFI Method

Demonstrated 3D system speed at the liquid-liquid interface	81 cm/hr
Demonstrated 3D resin speed at liquid-liquid interface	159 cm/hr
Maximum MakerJuice G+ resin print speed	160-180 cm/hr

APPENDIX 4

Examples of 3D Printed Parts

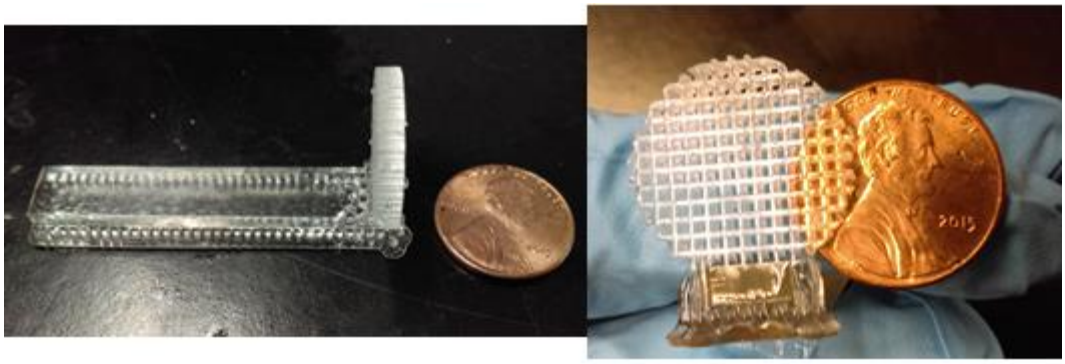

Figure 16: A 3D printed "slotted spoon" for scooping films from the liquid-liquid interface. Printed using Autodesk PR48 resin using the Ember printer in its factory default configuration (ie. not at a liquid-liquid interface).

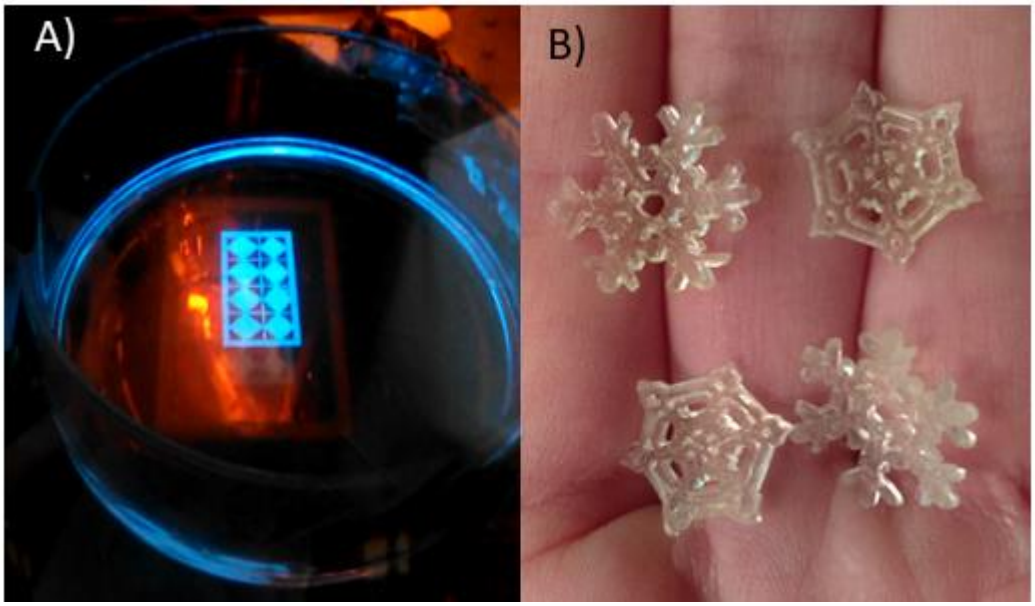

Figure 17: Thin films at the liquid-liquid interface. A) is an example of a sample used to generate the working curves during printing. Each diamond is exposed for a different, known length of

time and the cured height is measured. B) shows what happens when you've spent too many winters in Ithaca and can't think of anything besides snow as a demo print to show complexity and feature resolution.

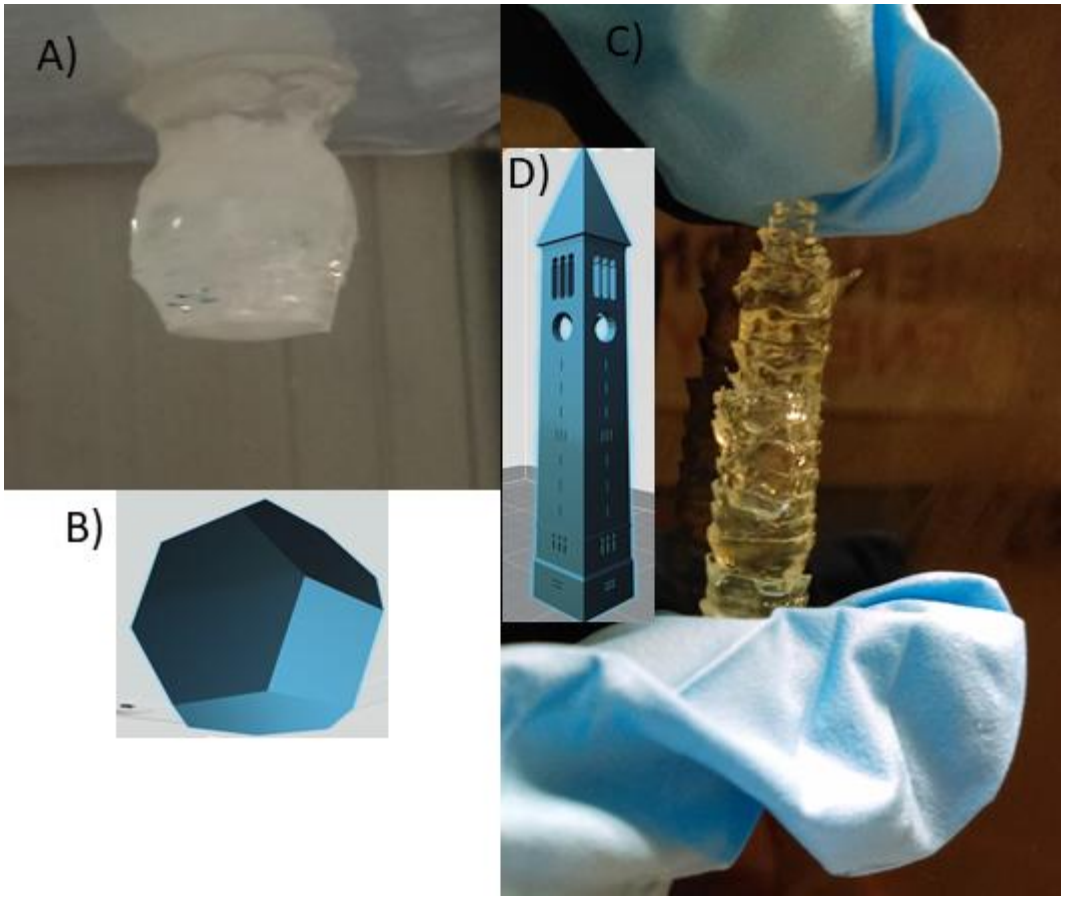

Figure 18: Examples of 3D parts printed at the liquid-liquid interface. A) is a 10 mm truncated octahedron printed with supports from Autodesk PR48 on HFE subphase. It would have ranked as a 4 quality and its CAD image is shown in B. C) shows a 20 mm tall McGraw Tower printed from MakerJuice resin with a large layer height as evidenced by the tapering between each jagged layer. This part printed in 2 minutes, giving a print rate of 600 mm/hr.

Figure 19: A model of a B2 printed with MakerJuice G+ resin on HFE-7200 with 50 µm slicing

REFERENCES

[1] C. V. Haynes, “Fluted Projectile Points: Their Age and Dispersion,” *Science (80-.).*, vol. 145, no. 3639, p. 1408 LP-1413, Sep. 1964.

[2] M. A. A. Khan, A. K. Sheikh, and B. S. Al-Shaer, *Evolution of Metal Casting Technologies—A Historical Perspective*. Springer, Cham, 2017.

[3] J.-Y. Lin, “Composite vertical and horizontal multi-station multi-axis NC machining apparatus,” 2017.

[4] I. Gibson, D. W. Rosen, and B. Stucker, *Additive manufacturing technologies: Rapid prototyping to direct digital manufacturing*, vol. 54. Springer New York, 2010.

[5] C. Hull, “Apparatus for production of three-dimensional objects by stereolithography,” US4575330 A, 1984.

[6] B. P. Conner *et al.*, “Making sense of 3-D printing: Creating a map of additive manufacturing products and services,” *Addit. Manuf.*, vol. 1–4, pp. 64–76, Oct. 2014.

[7] B. Berman, “3-D printing: The new industrial revolution,” *Bus. Horiz.*, vol. 55, no. 2, pp. 155–162, Mar. 2012.

[8] S. Wagner, “UK engineers speed 3d printing technology,” *Eng.*, vol. 10, 2010.

[9] V. Petrovic, J. Vicente Haro Gonzalez, O. Jordá Ferrando, J. Delgado Gordillo,

J. Ramón Blasco Puchades, and L. Portolés Griñan, “Additive layered manufacturing: sectors of industrial application shown through case studies,” *Int. J. Prod. Res.*, vol. 49, no. 4, pp. 1061–1079, Feb. 2011.

[10] R. G. McGrath, *The End of Competitive Advantage: How to Keep Your Strategy Moving as Fast as Your Business*. Boston: Harvard Business Review Press, 2013.

[11] B. Obama, “Remarks by the President in the State of the Union Address,” 2013.

[12] M. Vaezi, H. Seitz, and S. Yang, “A review on 3D micro-additive manufacturing technologies,” *Int. J. Adv. Manuf. Technol.*, vol. 67, no. 5–8, pp. 1721–1754, 2013.

[13] X. Yan and P. Gu, “A review of rapid prototyping technologies and systems,” *Comput. Des.*, vol. 28, no. 4, pp. 307–318, Apr. 1996.

[14] M. Feygin, A. Shkolnik, M. N. Diamond, and E. Dvorskiy, “Laminated object manufacturing system,” US08635506, 22-Apr-1996.

[15] B. C. Gross, J. L. Erkal, S. Y. Lockwood, C. Chen, and D. M. Spence, “Evaluation of 3D Printing and Its Potential Impact on Biotechnology and the Chemical Sciences,” *Anal. Chem.*, vol. 86, no. 7, pp. 3240–3253, Apr. 2014.

[16] M. M. N. S. Scott Crump, “Apparatus and method for creating three-dimensional objects,” US07429012, 1992.

[17] A. Bowyer and V. Olliver, “The Official History of the RepRap Project,” *All3DP*, 2016. [Online]. Available: https://all3dp.com/history-of-the-reprap-project/.

[18] C. Van Weeren, R.; Agarwala, M.; Jamalabad, V.; Bandyophadyay, A.; Vaidyanathan, R.; Langrana, N.; Safari, A.; Whalen, P.; Danforth, S.; Ballard, “Proceedings of the Solid Freeform Fabrication Symposium,” 1995, pp. 314–321.

[19] E. Becker, E. W, P. Hagmann, A. Maner, and D. Munchmeyer, “No microstructures with high aspect ratios and great structural heights by synchrotron radiation lithography, galvanoforming, and plastic moulding (LIGA process),” *Microelec Eng*, vol. 4, pp. 35–56, 1986.

[20] A. Perrot, D. Rangeard, and A. Pierre, “Structural built-up of cement-based materials used for 3D-printing extrusion techniques,” *Mater. Struct.*, vol. 49, no. 4, pp. 1213–1220, Apr. 2016.

[21] Z. G. Zhong, F. Li, and Z. M. Li, “Short Fiber Reinforced Composites for Fused Deposition Modeling,” *Mater. Sci. Eng. A*, vol. 301, no. 2, pp. 125–130, 2001.

[22] S. J. Leigh, R. J. Bradley, C. P. Purssell, D. R. Billson, and D. A. Hutchins, “A Simple, Low-Cost Conductive Composite Material for 3D Printing of Electronic Sensors,” *PLoS One*, vol. 7, no. 11, p. e49365, Nov. 2012.

[23] D. W. Hutmacher, M. Sittinger, and M. V Risbud, “Scaffold-based tissue engineering: rationale for computer-aided design and solid free-form fabrication systems,” *Trends Biotechnol.*, vol. 22, no. 7, pp. 354–362, Jul. 2004.

[24] M. D. Symes *et al.*, “Integrated 3D-printed reactionware for chemical synthesis and analysis,” *Nat. Chem.*, vol. 4, no. 5, pp. 349–354, May 2012.

[25] M. S. Mannoor *et al.*, “3D Printed Bionic Ears,” *Nano Lett.*, vol. 13, no. 6, pp. 2634–2639, Jun. 2013.

[26] P. J. Kitson, M. H. Rosnes, V. Sans, V. Dragone, and L. Cronin, “Configurable 3D-Printed millifluidic and microfluidic ‘lab on a chip’ reactionware devices,” *Lab Chip*, vol. 12, no. 18, p. 3267, Aug. 2012.

[27] M. D’Auria *et al.*, “3-D Printed Metal-Pipe Rectangular Waveguides,” *IEEE Trans. Components, Packag. Manuf. Technol.*, vol. 5, no. 9, pp. 1339–1349, Sep. 2015.

[28] “Dutch open ‘world’s first 3D-printed bridge’,” *Phys.org*, 2017. [Online]. Available: https://phys.org/news/2017-10-dutch-world-3d-printed-bridge.html. [Accessed: 19-Feb-2018].

[29] “XYZprinting da Vinci Mini Wireless 3D Printer Multi 3FM1WXUS00F,” *Best Buy*. [Online]. Available: https://www.bestbuy.com/site/xyzprinting-da-vinci-mini-wireless-3d-printer-black-orange/5624305.p?skuId=5624305&ref=212&loc=1&ksid=7a2441ed-372e-

4ec6-bed5-aef46bc15f4d&ksprof_id=8&ksaffcode=pg265671&ksdevice=c&lsft=ref:212,loc:2. [Accessed: 19-Feb-2018].

[30] "XYZ DaVinci miniMaker 3D Printer," *Staples*. [Online]. Available: https://www.staples.com/xyz-davinci-minimaker-3d-printer/product_2837262. [Accessed: 19-Feb-2018].

[31] "XYZprinting da Vinci miniMaker 3D Printer by Office Depot & OfficeMax." [Online]. Available: https://www.officedepot.com/a/products/583034/XYZprinting-da-Vinci-miniMaker-3D-Printer/. [Accessed: 19-Feb-2018].

[32] "TRONXY P802D LCD Screen 3D Printer Large Printing Area 220*220*180mm Acrylic Structure US Plug Black Great Gift," *Walmart.com*. [Online]. Available: https://www.walmart.com/ip/TRONXY-P802D-LCD-Screen-3D-Printer-Large-Printing-Area-220-220-180mm-Acrylic-Structure-US-Plug-Black-Great-Gift/792031186?wmlspartner=wlpa&selectedSellerId=15564&adid=22222222227121426591&wl0=&wl1=g&wl2=c&wl3=233725623019&wl4=pl. [Accessed: 19-Feb-2018].

[33] D. I. Wimpenny, P. M. Pandey, and L. J. Kumar, Eds., *Advances in 3D Printing & Additive Manufacturing Technologies*. Singapore: Springer Singapore, 2017.

[34] K. Upadhyay, R. Dwivedi, and A. K. Singh, “Determination and Comparison of the Anisotropic Strengths of Fused Deposition Modeling P400 ABS,” in *Advances in 3D Printing & Additive Manufacturing Technologies*, Singapore: Springer Singapore, 2017, pp. 9–28.

[35] J. von Neumann and A. W. Burks, “Theory of Self-Reproducing Autmata,” *University of Illinois Press*, Urbana and London, p. 1966.

[36] D. Colley, “Instant Prototypes,” *Mechanical Engineering*, vol. 110, no. 7, New York, pp. 68–70, Jul-1988.

[37] K. Subramanian, N. Vail, J. Barlow, and H. Marcus, “Selective laser sintering of alumina with polymer binders,” *Rapid Prototyp. J.*, vol. 1, no. 2, pp. 24–35, Jun. 1995.

[38] T. Atta, “Comparison between Selective Laser Melting (SLM) and Selective Laser Sintering (SLS),” *Green Mechanic*, 2016. [Online]. Available: http://www.green-mechanic.com/2016/12/comparison-between-selective-laser.html. [Accessed: 18-Feb-2018].

[39] F. Abe, K. Osakada, M. Shiomi, K. Uematsu, and M. Matsumoto, “The manufacturing of hard tools from metallic powders by selective laser melting,” *J. Mater. Process. Technol.*, vol. 111, no. 1–3, pp. 210–213, Apr. 2001.

[40] E. O. Olakanmi, R. F. Cochrane, and K. W. Dalgarno, “A review on selective laser sintering/melting (SLS/SLM) of aluminium alloy powders: Processing,

microstructure, and properties," *Prog. Mater. Sci.*, vol. 74, pp. 401–477, Oct. 2015.

[41] M. Molitch-Hou, "Boeing Talks 3D Printing for Aerospace," *Engineering.com*, 2017. [Online]. Available: https://www.engineering.com/3DPrinting/3DPrintingArticles/ArticleID/15475/Boeing-Talks-3D-Printing-for-Aerospace.aspx. [Accessed: 15-Feb-2018].

[42] "Boeing: Licensing Patents and Technology." [Online]. Available: http://www.boeing.com/company/key-orgs/licensing/patents-and-technology.page. [Accessed: 15-Feb-2018].

[43] R. Knight, J. Wright, J. Beaman, and D. Freitag, "Metal processing using selective laser sintering and hot isostatic pressing (SLS/HIP)," *Proc. SFF Symp.*, pp. 349–354, 1996.

[44] D. Herzog, V. Seyda, E. Wycisk, and C. Emmelmann, "Additive manufacturing of metals," *Acta Mater.*, vol. 117, pp. 371–392, Sep. 2016.

[45] X. Gong, T. Anderson, and K. Chou, "Review on Powder-Based Electron Beam Additive Manufacturing Technology," in *ASME/ISCIE 2012 International Symposium on Flexible Automation*, 2012, p. 507.

[46] T. DebRoy *et al.*, "Additive manufacturing of metallic components – Process, structure and properties," *Prog. Mater. Sci.*, vol. 92, pp. 112–224, Mar. 2018.

[47] L. E. Murr *et al.*, "Metal Fabrication by Additive Manufacturing Using Laser

and Electron Beam Melting Technologies," *J. Mater. Sci. Technol.*, vol. 28, no. 1, pp. 1–14, Jan. 2012.

[48] C. J. Smith, S. Tammas-Williams, E. Hernandez-Nava, and I. Todd, "Tailoring the thermal conductivity of the powder bed in Electron Beam Melting (EBM) Additive Manufacturing," *Sci. Rep.*, vol. 7, no. 1, p. 10514, Dec. 2017.

[49] John R. Tumbleston *et al.*, "Continuous liquid interface production of 3D objects," *Science (80-.).*, vol. 347, no. 6228, pp. 1349–1352, 2015.

[50] R. Janusziewicz, J. R. Tumbleston, A. L. Quintanilla, S. J. Mecham, and J. M. DeSimone, "Layerless fabrication with continuous liquid interface production.," *Proc. Natl. Acad. Sci. U. S. A.*, vol. 113, no. 42, pp. 11703–11708, Oct. 2016.

[51] S. Corbel, O. Dufaud, and T. Roques-Carmes, *Stereolithography*. 2011.

[52] T. H. Pang, "Stereolithography epoxy resin development: Accuracy and dimensional stability," *SFF Symp.*, pp. 11–26, 1993.

[53] R. He *et al.*, "Fabrication of complex-shaped zirconia ceramic parts via a DLP-stereolithography-based 3D printing method," *Ceram. Int.*, vol. 44, no. 3, pp. 3412–3416, Feb. 2018.

[54] J. Borrello and P. Backeris, "Rapid Prototyping Technologies," in *Rapid Prototyping in Cardiac Disease: 3D Printing the Heart*, K. M. Farooqi, Ed. Cham: Springer International Publishing, 2017, pp. 41–49.

[55] F. P. W. Melchels, J. Feijen, and D. W. Grijpma, “A review on stereolithography and its applications in biomedical engineering,” *Biomaterials*, vol. 31, no. 24, pp. 6121–6130, 2010.

[56] E. Matias and B. Rao, “3D printing: On its historical evolution and the implications for business,” *2015 Portl. Int. Conf. Manag. Eng. Technol.*, vol. 2015–Septe, pp. 551–558, 2015.

[57] “Google Scholar Search Results.” [Online]. Available: https://scholar.google.com/scholar?as_sdt=0,33&q=stereolithography&hl=en&as_ylo=2016&as_yhi=2017&as_vis=1.

[58] T. Takagi and N. Nakajima, “Photoforming applied to fine machining,” in *[1993] Proceedings IEEE Micro Electro Mechanical Systems*, pp. 173–178.

[59] A. Bertsch, S. Zissi, J. Y. Jézéquel, S. Corbel, and J. C. André, “Microstereophotolithography using a liquid crystal display as dynamic mask-generator,” *Microsyst. Technol.*, vol. 3, no. 2, pp. 42–47, Feb. 1997.

[60] C. Sun, N. Fang, D. M. Wu, and X. Zhang, “Projection micro-stereolithography using digital micro-mirror dynamic mask,” *Sensors Actuators A Phys.*, vol. 121, no. 1, pp. 113–120, May 2005.

[61] Texas Instruments, “DLP Products - Getting Started.” [Online]. Available: http://www.ti.com/dlp-chip/getting-started.html. [Accessed: 27-Feb-2018].

[62] R. E. Meier, “DMD pixel mechanics simulation,” *TI Tech. J.*, vol. 15, no. 3, pp.

64–74, 1998.

[63] D. E. Yunus, S. Sohrabi, R. He, W. Shi, and Y. Liu, “Acoustic patterning for 3D embedded electrically conductive wire in stereolithography,” *J. Micromechanics Microengineering*, vol. 27, no. 4, p. 45016, Apr. 2017.

[64] R. Sodian *et al.*, “Application of Stereolithography for Scaffold Fabrication for Tissue Engineered Heart Valves,” *ASAIO*, vol. 48, no. 1, pp. 12–16, 2002.

[65] P. J. Bártolo, Ed., *Stereolithography*. Boston, MA: Springer US, 2011.

[66] R. F. Shepherd, A. A. Stokes, R. M. D. Nunes, and G. M. Whitesides, “Soft Machines That are Resistant to Puncture and That Self Seal,” *Adv. Mater.*, vol. 25, no. 46, pp. 6709–6713, Dec. 2013.

[67] J. DeSimone, “What if 3D printing was 100x faster? | TED Talk,” *TedTalks*, 2015. [Online]. Available: https://www.ted.com/talks/joe_desimone_what_if_3d_printing_was_25x_faster. [Accessed: 09-Mar-2018].

[68] P. Palin, “How to Configure Ember for High Speed 3D Printing,” 2016. [Online]. Available: https://www.instructables.com/id/How-to-Configure-Ember-for-High-Speed-3D-Printing/. [Accessed: 08-Mar-2018].

[69] P. F. Jacobs, *Rapid Prototyping and Manufacturing: Fundamentals of Stereolithography*. New York: Society of Manufacturing Engineers, 1992.

[70] S. S. Labana and American Chemical Society., *Chemistry and properties of crosslinked polymers*. Academic Press, 1977.

[71] "Chain-Growth versus Step-Growth Polymerization," *Polymerdatabase.com*, 2015. [Online]. Available: http://polymerdatabase.com/polymer chemistry/Chain versus Step Growth.html. [Accessed: 27-Feb-2018].

[72] V. Shukla, M. Bajpai, D. K. Singh, M. Singh, and R. Shukla, "Review of basic chemistry of UV-curing technology," *Pigment Resin Technol.*, vol. 33, no. 5, pp. 272–279, Oct. 2004.

[73] S. C. Ligon, B. Husa, H. Wutzel, R. Holman, and R. Liska, "Strategies to Reduce Oxygen Inhibition in Photoinduced Polymerization," *ACS Chem. Rev.*, vol. 114, pp. 557–589, 2013.

[74] C. Decker and B. Elazouk, "Laser curing of photopolymers," in *Current trends in polymer photochemistry*, N. S. Allen, M. Edge, I. R. Bellobono, and E. Selli, Eds. New York: Prentice Hall, 1995, p. 130.

[75] J. Pelgrims, "Present Status of UV-curable coating technology in the United States," *J. Oil Coulour Chem. Assoc.*, vol. 61, no. 9, pp. 114–118, 1978.

[76] "Autodesk - Ember Tech Specs." [Online]. Available: https://ember.autodesk.com/overview#tech_specs. [Accessed: 28-Feb-2018].

[77] R. Domingo-Roca, B. Tiller, J. C. Jackson, and J. F. C. Windmill, "Bio-inspired 3D-printed piezoelectric device for acoustic frequency selection," *Sensors*

Actuators A Phys., vol. 271, pp. 1–8, Mar. 2018.

[78] F. J. Davis and G. R. Mitchell, "Polymeric Materials for Rapid Manufacturing," in *Stereolithography - Materials, Processes, and Applications*, P. J. Bartolo, Ed. 2011, pp. 113–141.

[79] W. F. Reed and A. M. Alb, *Monitoring polymerization reactions : from fundamentals to applications*. .

[80] J. J. Beaman, J. W. Barlow, D. L. Bourell, R. H. Crawford, H. L. Marcus, and K. P. McAlea, *Solid Freeform Fabrication: A New Direction in Manufacturing*. Boston, MA: Springer US, 1997.

[81] P. Calvert and R. Crockett, "Chemical Solid Free-Form Fabrication: Making Shapes without Molds," *Chem. Mater.*, vol. 9, no. 3, pp. 650–663, 1997.

[82] "Technical Documents – MakerJuice Labs." [Online]. Available: https://makerjuice.com/pages/technical-documents. [Accessed: 27-Feb-2018].

[83] "Autodesk Standard Clear Resin is now Open Source." [Online]. Available: http://learn.ember.autodesk.com/blog/open-source-resin. [Accessed: 27-Feb-2018].

[84] "MakerJuice G+ - Hard Multi-Purpose Resin." [Online]. Available: https://makerjuice.com/products/g. [Accessed: 27-Feb-2018].

[85] "Safety Data Sheets – Ember Support Center." [Online]. Available:

https://support.ember.autodesk.com/hc/en-us/articles/209662978-Safety-Data-Sheets-. [Accessed: 27-Feb-2018].

[86] J. V. Crivello and K. Dietliker, *Photoinitiators for free radical, cationic & anionic photopolymerisation*, 2nd ed. Chichester, West Sussex, England ; Wiley, 1998.

[87] P. F. Jacobs, *Stereolithography and other RP and M technologies : from rapid prototyping to rapid tooling*. Society of Manufacturing Engineers in cooperation with the Rapid Prototyping Association of SME, 1996.

[88] Y.-J. Park, D.-H. Lim, H.-J. Kim, D.-S. Park, and I.-K. Sung, "UV- and thermal-curing behaviors of dual-curable adhesives based on epoxy acrylate oligomers," *Int. J. Adhes. Adhes.*, vol. 29, no. 7, pp. 710–717, Oct. 2009.

[89] D. Calloway, "Beer-Lambert Law," *J. Chem. Educ.*, vol. 74, no. 7, p. 744, 1997.

[90] A. Reiser, *Photoreactive polymers: The science and technology of resists*. Wiley Subscription Services, Inc., A Wiley Company, 1989.

[91] K. Mostafa, A. J. Qureshi, and C. Montemagno, "Tolerance Control Using Subvoxel Gray-Scale DLP 3D Printing," in *Volume 2: Advanced Manufacturing*, 2017, p. V002T02A035.

[92] A. R. Johnson *et al.*, "Single-Step Fabrication of Computationally Designed Microneedles by Continuous Liquid Interface Production."

[93] P. F. Jacobs, “Solid Freeform Fabrication Proceedings: Fundamentals of Stereolithography,” 1992.

[94] S. A. Cinar, F. De Proft, D. Avci, V. Aviyente, and F. De Vleeschouwer, “Relationship Between the Free Radical Polymerization Rates of Methacrylates and the Chemical Properties of their Monomeric Radicals,” *Macromol. Chem. Phys.*, vol. 216, no. 3, pp. 334–343, Feb. 2015.

[95] Y. C. Kim *et al.*, “UV-curing kinetics and performance development of in situ curable 3D printing materials,” *Eur. Polym. J.*, vol. 93, pp. 140–147, Aug. 2017.

[96] B. Adzima, “The Ember Printer: An Open Platorm for Software, Hardware, and Materials Development.”

[97] M. W. Denny, *Air and Water: The Biology and Physics of Life’s Media*, 1st ed. Princeton: Princeton University Press, 1993.

[98] A. Vyatskikh, S. Delalande, A. Kudo, X. Zhang, C. M. Portela, and J. R. Greer, “Additive manufacturing of 3D nano-architected metals,” *Nat. Commun.*, vol. 9, no. 1, p. 593, Dec. 2018.

[99] H. Gong, B. P. Bickham, A. T. Woolley, and G. P. Nordin, “Custom 3D printer and resin for 18 μm × 20 μm microfluidic flow channels,” *Lab Chip*, vol. 17, no. 17, pp. 2899–2909, 2017.

[100] K. Rossmann, “Point Spread-Function, Line Spread-Function, and Modulation

Transfer Function," *Radiology*, vol. 93, no. 2, pp. 257–272, Aug. 1969.

[101] J. J. Choi *et al.*, "Controlling Nanocrystal Superlattice Symmetry and Shape-Anisotropic Interactions through Variable Ligand Surface Coverage," *J. Am. Chem. Soc.*, vol. 133, no. 9, pp. 3131–3138, Mar. 2011.

[102] J. Bennett, "Measuring UV curing parameters of commercial photopolymers used in additive manufacturing," *Addit. Manuf.*, 2017.

[103] "ENVIRONMENTAL FATE AND EFFECTS OF ETHYLENE GLYCOL USED AT AIRPORTS," 2000.

[104] I. Bravo, Y. Díaz-de-Mera, A. Aranda, K. Smith, K. P. Shine, and G. Marston, "Atmospheric chemistry of C4F9OC2H5 (HFE-7200), C4F9OCH3 (HFE-7100), C3F7OCH3 (HFE-7000) and C3F7CH2OH: temperature dependence of the kinetics of their reactions with OH radicals, atmospheric lifetimes and global warming potentials," *Phys. Chem. Chem. Phys.*, vol. 12, no. 19, p. 5115, May 2010.

[105] "Substance G+ Data Sheet: High Performance, General Purpose UV Cure Resin." MakerJuice, Overland Park.

[106] V. L. Thrumond, R. W. Potter, and M. A. Clynne, "The Densities of Saturated Solutions of NaCl and KCl from 10* to 105*C," in *United States Department of the Interior Geological Survey*, 1985.

[107] F. Á. Mohos, "Appendix 2: Solutions of Sucrose, Corn Syrup and other

Monosaccharides and Disaccharides," in *Confectionery and Chocolate Engineering*, Oxford, UK: Wiley-Blackwell, 2010, pp. 579–581.

[108] "HFE-7200 3M ™ Novec ™ Engineered Fluid MSDS." 3M Company, 2016.

[109] "Ethylene glycol | CH2OHCH2OH." [Online]. Available: https://pubchem.ncbi.nlm.nih.gov/compound/ethylene_glycol#section=Solubility. [Accessed: 06-Mar-2018].

[110] P.-G. de Gennes, F. Brochard-Wyart, and D. Quéré, *Capillarity and wetting phenomena : drops, bubbles, pearls, waves*. Springer, 2004.

[111] P. Ghosh, "Interfacial Tension." NPTEL Department of Chemical Engineering, Guwahati.

[112] A. Yoffe and E. Heymann, "Note on Antonoff's Rule.," *J. Phys. Chem.*, vol. 47, no. 5, pp. 409–410, May 1943.

[113] F. M. Fowkes, "ATTRACTIVE FORCES AT INTERFACES," *Ind. Eng. Chem.*, vol. 56, no. 12, pp. 40–52, Dec. 1964.

[114] A. D. Dussaud and S. M. Troian, "Dynamics of spontaneous spreading with evaporation on a deep fluid layer," *Phys. Fluids*, vol. 10, no. 1, p. 23, Jun. 1998.

[115] B. Steyrer, B. Busetti, G. Harakály, R. Liska, and J. Stampfl, "Hot Lithography vs. room temperature DLP 3D-printing of a dimethacrylate," *Addit. Manuf.*, vol. 21, pp. 209–214, May 2018.

[116] B. Benedict, “G Printer, Gooo3D’s UV DLP 3D printer can function without a PC or network,” *www.3ders.org*, 2015. [Online]. Available: https://www.3ders.org/articles/20151110-gooo3d-g-printer-uv-dlp-3d-printer-function-without-a-pc-or-network.html. [Accessed: 08-Apr-2018].